The Astrophysical Journal Supplement Series, 260:50 (23pp), 2022 June https://doi.org/10.3847/1538-4365/ac63ae

Large-scale Multiconfiguration Dirac–Hartree–Fock Calculations for Astrophysics: C-like Ions from O III to Mg VII

J. Q. Li[1], C. Y. Zhang[1,2], G. Del Zanna[3], P. Jönsson[4], M. Godefroid[5], G. Gaigalas[6], P. Rynkun[6], L. Radžiūtė[6], K. Wang[2], R. Si[1], and C. Y. Chen[1]

[1] Shanghai EBIT Lab, Key Laboratory of Nuclear Physics and Ion-beam Application, Institute of Modern Physics, Department of Nuclear Science and Technology, Fudan University, Shanghai 200433, People's Republic of China; rsi@fudan.edu, chychen@fudan.edu.cn

[2] Hebei Key Lab of Optic-electronic Information and Materials, The College of Physics Science and Technology, Hebei University, Baoding 071002, People's Republic of China; wang_kai10@fudan.edu.cn

[3] DAMTP, Centre for Mathematical Sciences, University of Cambridge, Wilberforce Road, Cambridge CB3 0WA, UK

[4] Group for Materials Science and Applied Mathematics, Malmö University, SE-20506, Malmö, Sweden

[5] Spectroscopy, Quantum Chemistry and Atmospheric Remote Sensing, CP160/09, Université libre de Bruxelles, B-1050 Brussels, Belgium

[6] Institute of Theoretical Physics and Astronomy, Vilnius University, Saulėtekio av. 3, LT-10257, Vilnius, Lithuania

Received 2021 November 22; revised 2022 March 21; accepted 2022 March 26; published 2022 June 23

Abstract

Large-scale multiconfiguration Dirac–Hartree–Fock calculations are provided for the $n \leqslant 5$ states in C-like ions from O III to Mg VII. Electron correlation effects are accounted for by using large configuration state function expansions, built from sets of orbitals with principal quantum numbers $n \leqslant 10$. An accurate and complete data set of excitation energies, wavelengths, radiative transition parameters, and lifetimes is offered for the 156 (196, 215, 272, 318) lowest states of the $2s^22p^2$, $2s2p^3$, $2p^4$, $2s^22p3s$, $2s^22p3p$, $2s^22p3d$, $2s2p^23s$, $2s2p^23p$, $2s2p^23d$, $2p^33s$, $2p^33p$, $2p^33d$, $2s^22p4s$, $2s^22p4p$, $2s^22p4d$, $2s^22p4f$, $2s2p^24s$, $2s2p^24p$, $2s2p^24d$, $2s2p^24f$, $2s^22p5s$, $2s^22p5p$, $2s^22p5d$, $2s^22p5f$, and $2s^22p5g$ configurations in O III (F IV, Ne V, Na VI, Mg VII). By comparing available experimental wavelengths with the MCDHF results, the previous line identifications for the $n = 5, 4, 3 \rightarrow n = 2$ transitions of Na VI in the X-ray and EUV wavelength range are revised. For several previous identifications discrepancies are found, and tentative new (or revised) identifications are proposed. A consistent atomic data set including both energy and transition data with spectroscopic accuracy is provided for the lowest hundreds of states for C-like ions from O III to Mg VII.

Unified Astronomy Thesaurus concepts: Atomic data benchmarking (2064); Laboratory astrophysics (2004)

Supporting material: machine-readable tables

1. Introduction

As the main source of cosmic information, atomic spectra play an indispensable role in studying the characteristics of various astrophysical objects. Advances in observational means and techniques have largely enriched telescope observations, which require a more accurate atomic line database as a reference, but unfortunately, there are many vacancies in the reference database (Delamere et al. 2005; Kallman & Palmeri 2007; Del Zanna & Mason 2018). To fill the gap between telescope observations and the reference database, we have performed state-of-the-art atomic calculations for L-shell atomic ions (Wang et al. 2014, 2015, 2016a, 2016b, 2017, 2018a, 2018b; Si et al. 2016, 2018; Song et al. 2021). An accurate data set of excitation energies, lifetimes, and transition rates for the states belonging to the $n \leqslant 5$ configurations of carbon-like ions from O III to Mg VII is provided in the present work.

Emission lines of these ions have been observed from different astrophysical objects, such as the Sun (Doschek & Bhatia 1990; Thomas & Neupert 1994; Curdt et al. 1997, 2001, 2004; Feldman et al. 1997, 2000; Brooks et al. 1999; Parenti et al. 2005; Tian et al. 2009; Del Zanna & Andretta 2011; Del Zanna & Woods 2013; Shestov et al. 2014), stars (Dean & Bruhweiler 1985; Raassen et al. 2002; Young et al. 2005, 2006), and planetary nebula (Forrest et al. 1980; Oliva et al. 1996; Feuchtgruber et al. 1997; McKenna et al. 1997; Sharpee et al. 2004; Young et al. 2011). They are used to determine the physical conditions in different astrophysical objects, such as temperature, density, and radiation field (Del Zanna & Woods 2013; Del Zanna & Mason 2018).

In the past decades, there were many atomic structure calculations involving low-lying states of the $n = 2$ and $n = 3$ configurations for C-like ions from O III to Mg VII (Fawcett 1987; Bhatia & Doschek 1993, 1995; Zhang & Sampson 1996; Aggarwal et al. 1997; Aggarwal & Keenan 1999; Aggarwal et al. 2001; Tachiev & Froese Fischer 2001; Froese Fischer & Tachiev 2004; Gu 2005; Safronova et al. 2006; Jönsson & Bieroń 2010; Jönsson et al. 2011; Liu et al. 2013; Zeng et al. 2017; Sun et al. 2018, 2020). For a review of scattering calculations, see the recent paper by Mao et al. (2020).

Spectral lines from higher-lying states are often observed from different astrophysical objects and laboratory plasmas (Raassen et al. 2002; Beiersdorfer & Träbert 2018). For example, lines from the $n > 3$ states of the light elements, such as oxygen, were identified in the spectra of the supergiant δ Orionis (Raassen & Pollock 2013). Therefore, there is a clear need for atomic data of the $n > 3$ higher-lying states. These data can be used to analyze new observations from different space missions and laboratory experiments (Träbert et al. 2014a, 2014b; Del Zanna & Mason 2018).

Using the multiconfiguration Hartree–Fock (MCHF) method in combination with B-spline expansions, Tayal & Zatsarinny (2017) performed calculations of excitation energies and transition probabilities for the 202 fine-structure states belonging to the $(1s^2)2s^22p^2$, $2s2p^3$, $2p^4$, $2s^22p3s$, $2s^22p3p$, $2s^22p3d$, $2s2p^23s$, $2s2p^23p$, $2s2p^23d$, $2s^22p4s$, $2s^22p4p$, $2s^22p4d$, $2s^22p4f$, and $2s^22p5s$ configurations in O III. Excitation energies and oscillator strengths for the $2s^22p^2$, $2s2p^3$, $2s^22p3s$, $2s^22p3p$, $2s^22p3d$, $2s^22p4s$, $2s^22p4p$, and $2s^22p5s$ configurations in C-like ions from N II to Ne V were provided by Al-Modlej et al. (2018), using three different codes, i.e., Cowan (1981), SUPERSTRUCTURE (Eissner et al. 1974), and AUTOSTRUCTURE (Badnell 1997).

Among previous theoretical studies relating to the $n > 3$ states for C-like ions from O III to Ne V, theoretical results provided by Tayal & Zatsarinny (2017) and Al-Modlej et al. (2018) are not accurate enough. For example, excitation energies of the $n > 3$ states in O III provided by Al-Modlej et al. (2018) depart from compiled results in the Atomic Spectra Database of the National Institute of Standard and Technology (hereafter referred to as the NIST database; Kramida et al. 2020) by up to 1%. Such uncertainty is too large for deblending and identification of new observations from various space missions (Del Zanna & Mason 2018). This issue will be discussed in detail in Section 3.1.

Using the multiconfiguration Dirac–Hartree–Fock method and the relativistic configuration interaction method (in the following referred to as MCDHF), excitation energies and lifetimes for the 156 (196, 215, 272, 318) lowest states of the $2s^22p^2$, $2s2p^3$, $2p^4$, $2s^22p3s$, $2s^22p3p$, $2s^22p3d$, $2s2p^23s$, $2s2p^23p$, $2s2p^23d$, $2p^33s$, $2p^33p$, $2p^33d$, $2s^22p4s$, $2s^22p4p$, $2s^22p4d$, $2s^22p4f$, $2s2p^24s$, $2s2p^24p$, $2s2p^24d$, $2s2p^24f$, $2s^22p5s$, $2s^22p5p$, $2s^22p5d$, $2s^22p5f$, and $2s^22p5g$ configurations in O III (F IV, Ne V, Na VI, Mg VII) are provided. The accuracy of the MCDHF results, excitation energies and transition rates, is carefully evaluated by employing comparisons with compiled data from the NIST database, analyzing convergence trends as the calculations are systematically enlarged, and comparing transition rates calculated in different forms, i.e., length and velocity forms. In Section 3.2, the identifications of the $n = 5$, 4, $3 \to n = 2$ transitions of Na VI will be reviewed. On the basis of the present MCDHF atomic data, some new line assignments of Na VI will be suggested. The comparisons, as well as the identification review of Na VI, offer a stringent accuracy assessment of the present MCDHF calculations.

2. Calculations and Results

The MCDHF method implemented in the GRASP2K code (Jönsson et al. 2013, 2007) was described by Froese Fischer et al. (2016) and was also introduced in our recent work (Wang et al. 2018a, 2018b; Song et al. 2021). Only computational procedures are provided here for this reason.

To generate configuration state function (CSF) expansions, the MCDHF calculations are performed separately for even and odd parities using an active space (AS) approach (Olsen et al. 1988; Sturesson et al. 2007). For different parities in the present MCDHF calculations, the multireference (MR) configurations include:

Even: $2s^22p^2$, $2p^4$, $2s^22p3p$, $2s2p^23s$, $2s2p^23d$, $2p^33p$, $2s^22p4p$, $2s^22p4f$, $2s2p^24s$, $2s2p^24d$, $2p^34p$, $2p^34f$, $2s^22p5p$, $2s^22p5f$, $2s2p^25s$, $2s2p^25d$, $2s2p^25g$, $2p^35p$, $2p^35f$;

Odd: $2s2p^3$, $2s^22p3s$, $2s^22p3d$, $2s2p^23p$, $2p^33s$, $2p^33d$, $2s^22p4s$, $2s^22p4d$, $2s2p^24p$, $2s2p^24f$, $2p^34s$, $2p^34d$, $2s^22p5s$, $2s^22p5d$, $2s^22p5g$, $2s2p^25p$, $2s2p^25f$, $2p^35s$, $2p^35d$, $2p^35g$.

The $n \leqslant 5$ orbitals for the even and odd parity states are determined simultaneously in EOL Dirac–Fock calculations (Dyall et al. 1989). By allowing single and double substitutions from all the $2 \leqslant n \leqslant 5$ electrons of the MR configurations to the active set (AS) of orbitals, as well as single substitutions from the $1s$ electrons, the CSF expansions are obtained. For the first step of the MCDHF calculations, the AS is defined as:

$AS_1 = \{6s, 6p, 6d, 6f, 6g, 6h\}$.

Then, the additional AS are defined in the following way:

$AS_2 = AS_1 + \{7s, 7p, 7d, 7f, 7g, 7h, 7i\}$,

$AS_3 = AS_2 + \{8s, 8p, 8d, 8f, 8g, 8h, 8i\}$,

$AS_4 = AS_3 + \{9s, 9p, 9d, 9f, 9g, 9h, 9i\}$,

$AS_5 = AS_4 + \{10s, 10p, 10d, 10f, 10g, 10h, 10i\}$.

The AS is enlarged layer by layer, which makes it possible to monitor the convergence of the results. In each step only the new layer of orbitals is optimized, keeping the previous layers fixed. The numbers of CSFs using the AS_5 active set are about 9.1 million for even parity, and 9.5 million for odd parity.

The transverse photon interaction in the low-frequency limit, as well as the leading quantum electrodynamic effects (self-energy and vacuum polarization), are added to the relativistic configuration interaction (RCI) calculations following the MCDHF orbital optimization. A transformation method from *jj*-coupled CSFs to *LSJ*-coupled CSFs (Gaigalas et al. 2017) is used to provide the atomic state functions in the *LSJ* labeling system.

Electron correlation is relatively more important for lower charged ions than for higher charged ions. Therefore, the convergence of the present MCDHF excitation energies is assessed by taking O III as an example. In Table 1, the MCDHF excitation energies as a function of the AS are present for the 156 states of O III. The compiled values from the NIST database (Kramida et al. 2020) are also provided for comparison. The mean difference with the standard deviation (defined as formulas (3) and (4) in Wang et al. 2017) between MCDHF and NIST values are $-686 \pm 958\ \mathrm{cm}^{-1}$, $-194 \pm 334\ \mathrm{cm}^{-1}$, $-94 \pm 201\ \mathrm{cm}^{-1}$, $-54 \pm 162\ \mathrm{cm}^{-1}$, and $-27 \pm 156\ \mathrm{cm}^{-1}$ for the calculations of the AS_1, AS_2, AS_3, AS_4, and AS_5, respectively. This comparison shows that with an increasing size of the AS, the MCDHF calculations are well converged. The remaining energy differences are caused by higher-order correlation effects, not captured within the framework of single and double substitutions from the MR.

The present MCDHF excitation energies (E_{MCDHF}) and lifetimes (τ^l_{MCDHF} in the length form and τ^v_{MCDHF} in the velocity form) of the 156 (196, 215, 272, 318) lowest states of the $2s^22p^2$, $2s2p^3$, $2p^4$, $2s^22p3s$, $2s^22p3p$, $2s^22p3d$, $2s2p^23s$, $2s2p^23p$, $2s2p^23d$, $2p^33s$, $2p^33p$, $2p^33d$, $2s^22p4s$, $2s^22p4p$, $2s^22p4d$, $2s^22p4f$, $2s2p^24s$, $2s2p^24p$, $2s2p^24d$, $2s2p^24f$, $2s^22p5s$, $2s^22p5p$, $2s^22p5d$, $2s^22p5f$, and $2s^22p5g$ configurations in O III (F IV, Ne V, Na VI, Mg VII) are provided in Table 2. Excitation energies E_{NIST} from the NIST database, as well as the energy differences $\Delta E = E_{\mathrm{MCDHF}} - E_{\mathrm{NIST}}$, are also provided in this table.

Table 1
The MCDHF Excitation Energies as a Function of the AS for the 156 States of O III

Key	Level	E_{MCDHF}					E_{NIST}	ΔE
		AS$_1$	AS$_2$	AS$_3$	AS$_4$	AS$_5$		
1	$2s^22p^2\ ^3P_0$	0	0	0	0	0	0	0
2	$2s^22p^2\ ^3P_1$	108.97	109.90	110.20	110.40	110.60	113.178	−2.578
3	$2s^22p^2\ ^3P_2$	296.71	300.83	302.16	302.91	303.54	306.174	−3
4	$2s^22p^2\ ^1D_2$	20,950.9	20,509.9	20,393.0	20,363.7	20,351.7	20,273.27	78
5	$2s^22p^2\ ^1S_0$	44,381.8	43,599.6	43,407.9	43,347.9	43,324.2	43,185.74	138
6	$2s2p^3\ ^5S_2^{\circ}$	59,242.1	60,047.7	60,180.6	60,218.7	60,255.9	60,324.79	−69
7	$2s2p^3\ ^3D_3^{\circ}$	120,751	120,288	120,189	120,166	120,185	120,025.2	160
8	$2s2p^3\ ^3D_2^{\circ}$	120,773	120,311	120,212	120,190	120,208	120,053.4	155
9	$2s2p^3\ ^3D_1^{\circ}$	120,777	120,316	120,218	120,196	120,214	120,058.2	156
10	$2s2p^3\ ^3P_2^{\circ}$	143,713	142,822	142,645	142,594	142,601	142,381.0	220
11	$2s2p^3\ ^3P_1^{\circ}$	143,710	142,822	142,647	142,596	142,603	142,381.8	221
12	$2s2p^3\ ^3P_0^{\circ}$	143,728	142,846	142,673	142,622	142,629	142,393.5	236
13	$2s2p^3\ ^1D_2^{\circ}$	189,458	187,759	187,476	187,413	187,422	187,054.0	368
14	$2s2p^3\ ^3S_1^{\circ}$	199,117	197,624	197,418	197,381	197,401	197,087.7	313
15	$2s2p^3\ ^1P_1^{\circ}$	213,247	211,342	211,009	210,923	210,920	210,461.8	458
16	$2s^22p3s\ ^3P_0^{\circ}$	266,279	266,893	267,038	267,100	267,120	267,258.71	−139
17	$2s^22p3s\ ^3P_1^{\circ}$	266,394	267,006	267,151	267,212	267,233	267,377.11	−144
18	$2s^22p3s\ ^3P_2^{\circ}$	266,649	267,261	267,407	267,469	267,491	267,634.00	−143
19	$2s^22p3s\ ^1P_1^{\circ}$	272,444	272,818	272,907	272,953	272,971	273,081.33	−110
20	$2p^4\ ^3P_2$	285,721	284,433	284,203	284,166	284,208	283,759.70	448
21	$2p^4\ ^3P_1$	285,923	284,647	284,418	284,382	284,425	283,977.40	448
22	$2p^4\ ^3P_0$	286,023	284,759	284,533	284,498	284,541	284,071.90	469
23	$2s^22p3p\ ^1P_1$	289,878	290,590	290,753	290,806	290,832	290,958.25	−126
24	$2s^22p3p\ ^3D_1$	292,857	293,528	293,675	293,721	293,741	293,866.49	−125
25	$2s^22p3p\ ^3D_2$	292,993	293,665	293,813	293,859	293,879	294,002.86	−124
26	$2s^22p3p\ ^3D_3$	293,212	293,887	294,037	294,083	294,103	294,223.07	−120
27	$2s^22p3p\ ^3S_1$	296,507	297,191	297,348	297,402	297,426	297,558.66	−133
28	$2p^4\ ^1D_2$	299,426	299,256	298,936	298,874	298,908	298,294.0	614
29	$2s^22p3p\ ^3P_0$	299,220	299,894	300,046	300,101	300,128	300,229.93	−102
30	$2s^22p3p\ ^3P_1$	299,299	299,972	300,124	300,179	300,206	300,311.96	−106
31	$2s^22p3p\ ^3P_2$	301,065	300,102	300,255	300,310	300,337	300,442.55	−106
32	$2s^22p3p\ ^1D_2$	305,964	306,464	306,519	306,532	306,543	306,586.08	−43
33	$2s^22p3p\ ^1S_0$	313,752	313,940	313,864	313,836	313,831	313,802.77	28
34	$2s^22p3d\ ^3F_2^{\circ}$	323,933	324,376	324,416	324,423	324,423	324,464.88	−42
35	$2s^22p3d\ ^3F_3^{\circ}$	324,210	324,616	324,641	324,639	324,634	324,660.80	−27
36	$2s^22p3d\ ^1D_2^{\circ}$	324,182	324,633	324,684	324,693	324,694	324,735.65	−42
37	$2s^22p3d\ ^3F_4^{\circ}$	324,397	324,814	324,839	324,833	324,825	324,839.03	−14
38	$2s^22p3d\ ^3D_1^{\circ}$	326,573	327,077	327,143	327,161	327,167	327,229.25	−62
39	$2s^22p3d\ ^3D_2^{\circ}$	326,626	327,135	327,200	327,215	327,220	327,278.30	−58
40	$2s^22p3d\ ^3D_3^{\circ}$	326,706	327,224	327,287	327,299	327,300	327,352.17	−52
41	$2s^22p3d\ ^3P_2^{\circ}$	328,764	329,302	329,383	329,403	329,409	329,469.80	−61
42	$2s^22p3d\ ^3P_1^{\circ}$	328,869	329,399	329,483	329,508	329,517	329,583.89	−67
43	$2s^22p3d\ ^3P_0^{\circ}$	328,928	329,457	329,543	329,571	329,582	329,645.14	−63
44	$2s^22p3d\ ^1F_3^{\circ}$	331,486	331,841	331,853	331,838	331,825	331,821.44	4
45	$2s^22p3d\ ^1P_1^{\circ}$	332,287	332,680	332,738	332,747	332,748	332,778.94	−31
46	$2s2p^2(^3P)3s\ ^5P_1$	337,070	338,067	338,279	338,368	338,427	338,577.25	−150
47	$2s2p^2(^3P)3s\ ^5P_2$	337,195	338,191	338,403	338,493	338,551	338,701.98	−151
48	$2s2p^2(^3P)3s\ ^5P_3$	337,357	338,354	338,567	338,657	338,716	338,863.03	−147
49	$2p^4\ ^1S_0$	347,270	344,709	344,246	344,135	344,147	343,306.3	841
50	$2s2p^2(^3P)3s\ ^3P_0$	349,192	349,831	349,905	349,952	349,990	350,024.49	−34
51	$2s2p^2(^3P)3s\ ^3P_1$	349,289	349,929	350,002	350,050	350,088	350,124.45	−36
52	$2s2p^2(^3P)3s\ ^3P_2$	349,460	350,101	350,175	350,223	350,261	350,298.38	−37
53	$2s^22p4s\ ^3P_0^{\circ}$	355,632	356,380	356,550	356,615	356,640	356,736.30	−96
54	$2s^22p4s\ ^3P_1^{\circ}$	355,740	356,485	356,655	356,719	356,744	356,844.98	−101
55	$2s^22p4s\ ^3P_2^{\circ}$	356,006	356,753	356,925	356,991	357,016	357,117.01	−101
56	$2s^22p4s\ ^1P_1^{\circ}$	357,894	358,463	358,577	358,620	358,634	358,668.90	−35
57	$2s2p^2(^3P)3p\ ^3S_1^{\circ}$	361,908	362,823	363,029	363,106	363,163	363,263.38	−100
58	$2s2p^2(^3P)3p\ ^5D_0^{\circ}$	364,137	365,087	365,295	365,365	365,416	365,527.08	−111
59	$2s2p^2(^3P)3p\ ^5D_1^{\circ}$	364,170	365,120	365,328	365,398	365,449	365,561.95	−113
60	$2s2p^2(^3P)3p\ ^5D_2^{\circ}$	364,238	365,188	365,397	365,467	365,518	365,630.40	−112
61	$2s^22p4p\ ^1P_1$	364,485	365,292	365,493	365,566	365,598	365,726.76	−129
62	$2s2p^2(^3P)3p\ ^5D_3^{\circ}$	364,339	365,291	365,501	365,571	365,622	365,730.68	−109
63	$2s2p^2(^3P)3p\ ^5D_4^{\circ}$	364,466	365,422	365,633	365,702	365,754	365,857.89	−104

Table 1
(Continued)

Key	Level	$E_{\rm MCDHF}$					$E_{\rm NIST}$	ΔE
		AS$_1$	AS$_2$	AS$_3$	AS$_4$	AS$_5$		
64	$2s^22p4p\ ^3D_1$	365,342	366,108	366,287	366,350	366,377	366,488.45	−111
65	$2s^22p4p\ ^3D_2$	365,450	366,217	366,396	366,458	366,485	366,595.76	−111
66	$2s^22p4p\ ^3D_3$	365,654	366,423	366,604	366,666	366,694	366,802.62	−109
67	$2s^22p4p\ ^3S_1$	366,886	367,630	367,790	367,845	367,869	367,953.90	−85
68	$2s2p^2(^3P)3p\ ^5P_1°$	367,117	368,067	368,282	368,360	368,415	368,538.65	−124
69	$2s2p^2(^3P)3p\ ^5P_2°$	367,173	368,124	368,339	368,417	368,472	368,595.93	−124
70	$2s2p^2(^3P)3p\ ^5P_3°$	367,274	368,227	368,442	368,520	368,576	368,697.00	−121
71	$2s^22p4p\ ^3P_0$	369,878	370,409	370,431	370,427	370,426	370,329.18	97
72	$2s^22p4p\ ^3P_1$	369,958	370,492	370,515	370,510	370,510	370,418.32	92
73	$2s^22p4p\ ^3P_2$	370,068	370,603	370,625	370,620	370,619	370,526.49	93
74	$2s^22p4p\ ^1D_2$	370,552	371,039	371,043	371,021	371,012	370,902.22	110
75	$2s^22p4p\ ^1S_0$	374,540	374,625	374,412	374,291	374,237		
76	$2s2p^2(^3P)3p\ ^3D_1°$	373,603	374,336	374,451	374,491	374,531	374,571.64	−41
77	$2s2p^2(^3P)3p\ ^3D_2°$	373,695	374,427	374,542	374,582	374,622	374,663.52	−42
78	$2s2p^2(^3P)3p\ ^3D_3°$	373,828	374,560	374,675	374,716	374,757	374,795.14	−38
79	$2s2p^2(^3P)3p\ ^5S_2°$	374,710	375,708	375,891	375,959	376,016	376,079.92	−64
80	$2s^22p4d\ ^3F_2°$	376,252	376,982	377,159	377,227	377,259	377,385.58	−127
81	$2s^22p4d\ ^3F_3°$	376,445	377,171	377,345	377,411	377,440	377,562.31	−122
82	$2s^22p4d\ ^1D_2°$	376,525	377,277	377,460	377,530	377,562	377,686.83	−125
83	$2s^22p4d\ ^3F_4°$	376,631	377,363	377,536	377,601	377,630	377,748.57	−119
84	$2s^22p4d\ ^3P_2°$	377,398	378,094	378,231	378,284	378,320	378,405.68	−86
85	$2s^22p4d\ ^3P_1°$	377,427	378,115	378,248	378,301	378,337	378,417.84	−81
86	$2s2p^2(^3P)3p\ ^3P_0°$	377,457	378,142	378,273	378,325	378,362	378,435.16	−73
87	$2s^22p4d\ ^3D_1°$	378,182	378,881	379,040	379,100	379,128	379,227.15	−99
88	$2s^22p4d\ ^3D_2°$	378,248	378,951	379,108	379,167	379,195	379,293.03	−98
89	$2s^22p4d\ ^3D_3°$	378,313	379,020	379,177	379,235	379,261	379,356.75	−96
90	$2s^22p4f\ ^3F_2$	379,239	380,176	380,423	380,505	380,530	380,621.90	−92
91	$2s^22p4f\ ^1F_3$	379,226	380,164	380,415	380,503	380,532	380,612.20	−80
92	$2s^22p4f\ ^3F_3$	379,287	380,223	380,470	380,553	380,578	380,671.30	−93
93	$2s^22p4f\ ^3F_4$	379,303	380,241	380,492	380,581	380,610	380,685.90	−76
94	$2s2p^2(^3P)3p\ ^3P_2°$	380,001	380,574	380,651	380,680	380,704	380,706.51	−3
95	$2s2p^2(^3P)3p\ ^3P_1°$	379,993	380,569	380,653	380,685	380,709	380,717.92	−9
96	$2s^22p4d\ ^3P_0°$	380,004	380,588	380,674	380,707	380,732	380,737.00	−5
97	$2s^22p4d\ ^1F_3°$	380,072	380,601	380,707	380,737	380,746	380,782.17	−36
98	$2s^22p4d\ ^1P_1°$	380,334	380,879	381,004	381,043	381,057	381,089.27	−32
99	$2s^22p4f\ ^3G_3$	379,808	380,741	380,987	381,068	381,092	381,176.90	−85
100	$2s^22p4f\ ^3G_4$	379,845	380,778	381,027	381,114	381,142	381,211.30	−69
101	$2s^22p4f\ ^3G_5$	380,038	380,971	381,222	381,310	381,339	381,404.50	−66
102	$2s^22p4f\ ^3D_3$	380,057	380,994	381,245	381,334	381,365	381,456.80	−92
103	$2s^22p4f\ ^3D_2$	380,084	381,018	381,265	381,348	381,375	381,477.80	−103
104	$2s^22p4f\ ^1G_4$	380,114	381,043	381,288	381,369	381,393	381,472.50	−80
105	$2s^22p4f\ ^3D_1$	380,224	381,161	381,410	381,494	381,522	381,623.80	−102
106	$2s^22p4f\ ^1D_2$	380,251	381,186	381,438	381,526	381,557	381,645.00	−88
107	$2s^22p5s\ ^3P_0°$	390,610	391,427	391,628	391,705	391,736	391,830.76	−95
108	$2s^22p5s\ ^3P_1°$	390,701	391,514	391,714	391,790	391,821	391,917.80	−97
109	$2s^22p5s\ ^3P_2°$	390,980	391,798	392,001	392,078	392,110	392,209.53	−100
110	$2s^22p5s\ ^1P_1°$	391,742	392,485	392,663	392,728	392,753	392,781.47	−28
111	$2s2p^2(^1D)3s\ ^3D_1$	393,282	393,857	393,975	394,031	394,069	394,079.4	−10
112	$2s2p^2(^1D)3s\ ^3D_2$	393,354	393,917	394,030	394,085	394,123	394,127.3	−4
113	$2s2p^2(^1D)3s\ ^3D_3$	393,461	394,010	394,118	394,172	394,209	394,197.9	11
114	$2s2p^2(^3P)3d\ ^5F_1$	393,509	394,292	394,391	394,424	394,462	394,528.20	−66
115	$2s2p^2(^3P)3d\ ^5F_2$	393,549	394,333	394,434	394,466	394,503	394,567.05	−64
116	$2s2p^2(^3P)3d\ ^5F_3$	393,609	394,398	394,500	394,531	394,567	394,624.68	−58
117	$2s2p^2(^3P)3d\ ^5F_4$	393,689	394,483	394,588	394,619	394,654	394,700.27	−46
118	$2s2p^2(^3P)3d\ ^5F_5$	393,785	394,586	394,694	394,724	394,757	394,793.28	−36
119	$2s^22p5p\ ^1P_1$	394,759	395,627	395,854	395,939	395,976		
120	$2s^22p5p\ ^3S_1$	395,932	396,758	396,954	397,024	397,054		
121	$2s^22p5p\ ^1D_2$	396,853	397,755	397,867	397,892	397,904		
122	$2s^22p5p\ ^3P_0$	396,865	397,754	397,871	397,900	397,909		
123	$2s^22p5p\ ^3P_1$	396,859	397,755	397,915	397,979	397,990		
124	$2s2p^2(^3P)3d\ ^5D_2$	397,147	397,769	397,917	397,983	398,038	398,139.92	−102
125	$2s2p^2(^3P)3d\ ^5D_1$	397,129	397,838	397,952	397,984	398,039	398,144.29	−105

Table 1
(Continued)

Key	Level	E_{MCDHF}					E_{NIST}	ΔE
		AS$_1$	AS$_2$	AS$_3$	AS$_4$	AS$_5$		
126	$2s2p^2(^3P)3d\ ^5D_0$	397,045	397,762	397,920	397,988	398,045	398,145.63	−101
127	$2s2p^2(^3P)3d\ ^5D_3$	396,858	397,771	397,933	397,999	398,052	398,150.40	−98
128	$2s2p^2(^3P)3d\ ^5D_4$	396,956	397,859	398,022	398,087	398,140	398,231.48	−91
129	$2s^22p5p\ \ ^3P_2$	397,190	397,991	398,105	398,134	398,144		
130	$2s^22p5p\ \ ^3D_1$	397,223	398,184	398,244	398,264	398,278		
131	$2s^22p5p\ \ ^3D_2$	397,315	398,150	398,320	398,363	398,378		
132	$2s2p^2(^3P)3d\ ^5P_3$	397,129	398,088	398,259	398,327	398,382	398,487.08	−105
133	$2s2p^2(^3P)3d\ ^5P_2$	397,901	398,288	398,344	398,393	398,450	398,557.17	−107
134	$2s^22p5p\ \ ^3D_3$	397,972	398,364	398,418	398,441	398,457		
135	$2s2p^2(^3P)3d\ ^5P_1$	397,830	398,198	398,356	398,428	398,486	398,595.65	−110
136	$2s2p^2(^3P)3d\ ^3P_2$	399,257	400,032	400,176	400,235	400,289	400,351.56	−63
137	$2s2p^2(^3P)3d\ ^3P_1$	399,368	400,147	400,292	400,350	400,402	400,460.99	−59
138	$2s2p^2(^3P)3d\ ^3P_0$	399,428	400,211	400,357	400,415	400,466	400,514.89	−49
139	$2s^22p5p\ \ ^1S_0$	401,971	401,785	401,419	401,210	401,102		
140	$2s2p^2(^3P)3d\ ^3F_2$	400,571	401,234	401,306	401,322	401,349	401,375.09	−26
141	$2s^22p5d\ \ ^3F_2^{\circ}$	400,190	401,035	401,260	401,347	401,386	401,519.8	−134
142	$2s2p^2(^3P)3d\ ^3F_3$	400,672	401,332	401,403	401,420	401,448	401,476.29	−28
143	$2s^22p5d\ \ ^3F_3^{\circ}$	400,369	401,210	401,433	401,519	401,557	401,725.6	−169
144	$2s2p^2(^3P)3d\ ^3F_4$	400,802	401,460	401,530	401,549	401,578	401,605.52	−28
145	$2s^22p5d\ \ ^1D_2^{\circ}$	400,452	401,305	401,533	401,620	401,659	401,791.7	−133
146	$2s^22p5d\ \ ^3F_4^{\circ}$	400,569	401,414	401,639	401,725	401,763	401,893.2	−130
147	$2s^22p5d\ \ ^3D_1^{\circ}$	401,073	401,892	402,109	402,192	402,229		
148	$2s^22p5d\ \ ^3D_2^{\circ}$	401,123	401,946	402,163	402,246	402,283	402,411.5	−129
149	$2s^22p5d\ \ ^3D_3^{\circ}$	401,240	402,064	402,281	402,364	402,401	402,533.3	−132
150	$2s^22p5d\ \ ^3P_2^{\circ}$	401,490	402,310	402,524	402,606	402,642		
151	$2s^22p5d\ \ ^3P_1^{\circ}$	401,563	402,381	402,596	402,679	402,715		
152	$2s^22p5d\ \ ^3P_0^{\circ}$	401,602	402,421	402,637	402,721	402,757		
153	$2s^22p5f\ \ ^1F_3$	401,758	402,699	402,952	403,043	403,077		
154	$2s^22p5f\ \ ^3F_2$	401,780	402,716	402,966	403,054	403,086		
155	$2s^22p5f\ \ ^3F_3$	401,797	402,734	402,984	403,073	403,105		
156	$2s^22p5f\ \ ^3F_4$	401,823	402,759	403,011	403,102	403,136		

Note. The compiled values from the NIST database (Kramida et al. 2020) are also provided for comparison. E_{MCDHF} (AS$_1$, AS$_2$, AS$_3$, AS$_4$, and AS$_5$): the present MCDHF excitation energies in cm^{-1}; E_{NIST}: the compiled values in cm^{-1} from the NIST database (Kramida et al. 2020); ΔE: the differences (E_{MCDHF} (AS$_5$) − E_{NIST}) between the MCDHF calculated values for AS$_5$ and the compiled values from the NIST database.

In Table 3, wavelengths λ and radiative transition parameters (transition rates A, weighted oscillator strengths gf, line strengths S) for electric dipole (E1), electric quadrupole (E2), magnetic dipole (M1), and magnetic quadrupole (M2) transitions among all the states listed in Table 2 are provided, as well as branching fractions ($\mathrm{BF}_{ji} = A_{ji} / \sum_{k=1}^{j-1} A_{jk}$). Radiative transition parameters in both the length (l) and velocity (v) forms (corresponding to Babushkin and Coulomb gauges) from the present MCDHF calculations using the AS_5 space are provided, as well as those in the length (l) form from the present MCDHF calculations using the AS_4 space. To reduce the amount of data, only transitions with radiative branching fractions (BF) larger than 10^{-5} are provided.

3. Evaluation of Data

3.1. Energy Levels

Among C-like ions from O III to Mg VII, both theoretical and experimental excitation energies of O III are relatively complete. In Table 4, we evaluate the accuracy of the present MCDHF excitation energies of O III by comparing them with available data, including the calculations by Jönsson & Bieroń (2010), Jönsson et al. (2011) (hereafter referred to as MCDHF1), by Tachiev & Froese Fischer (2001), Froese Fischer & Tachiev (2004) (MCHF), by Tayal & Zatsarinny (2017) (MCHF1), and by Al-Modlej et al. (2018) (AUTOSTRUCTURE) and the compiled values from the NIST database (Kramida et al. 2020). The compiled values from the NIST database were derived by Pettersson (1982) based on their observed lines from a theta-pinch discharge as a light source, which were measured between 500 and 8500 Å. The accuracy for the lines in the region below 2200 Å is estimated to be about 0.01 Å. In the region 2000–7000 Å, the wavelength values are believed to be accurate to better than 0.03 Å. Above 7000 Å the accuracy is about 0.1 Å.

Theoretical values for the 15 lowest states of the $2s^22p^2$ and $2s2p^3$ configurations are provided by all the above calculations. The average difference with the standard deviation with the compiled values from the NIST database are 162 ± 148 cm^{-1} for MCDHF, 153 ± 220 cm^{-1} for MCDHF1, 341 ± 248 cm^{-1} for MCHF, 164 ± 195 cm^{-1} for MCHF1, and 1267 ± 7542 cm^{-1} for AUTOSTRUCTURE. The accuracies of the three calculations (MCDHF, MCDHF1, MCHF1) are generally at the same level, which are better than those of the MCHF and AUTOSTRUCTURE calculations.

As shown in Table 4, the present MCDHF calculations, as well as MCHF, MCHF1, and AUTOSTRUCTURE provide excitation energies of higher states (above the state with the key

Table 2
Excitation Energies (in cm^{-1}) and Radiative Lifetimes (in seconds) for the 156 (196, 215, 272, 318) Lowest States of the $n \leqslant 5$ States in O III (F IV, Ne V, Na VI, Mg VII)

Z	Key	Level	E_{MCDHF}	E_{NIST}	ΔE	$\tau^{l}_{\mathrm{MCDHF}}$	$\tau^{v}_{\mathrm{MCDHF}}$	LS Composition
8	1	$2s^22p^2\ {}^3P_0$	0	0	0			0.95
8	2	$2s^22p^2\ {}^3P_1$	110.60	113.178	−2.578	4.112E+04	4.112E+04	0.95
8	3	$2s^22p^2\ {}^3P_2$	303.54	306.174	−2.634	1.033E+04	1.033E+04	0.95
8	4	$2s^22p^2\ {}^1D_2$	20,351.7	20,273.27	78.43	3.637E+01	3.638E+01	0.94
8	5	$2s^22p^2\ {}^1S_0$	43,324.2	43,185.74	138.46	5.152E-01	5.184E-01	0.90+0.06 $2p^4\ {}^1S$
8	6	$2s2p^3\ {}^5S_2^\circ$	60,255.9	60,324.79	−68.89	1.288E-03	6.337E-04	0.98
8	7	$2s2p^3\ {}^3D_3^\circ$	120,185	120,025.2	159.8	1.618E-09	1.613E-09	0.94
8	8	$2s2p^3\ {}^3D_2^\circ$	120,208	120,053.4	154.6	1.610E-09	1.608E-09	0.94
8	9	$2s2p^3\ {}^3D_1^\circ$	120,214	120,058.2	155.8	1.604E-09	1.604E-09	0.94
8	10	$2s2p^3\ {}^3P_2^\circ$	142,601	142,381.0	220	5.416E-10	5.449E-10	0.94
8	11	$2s2p^3\ {}^3P_1^\circ$	142,603	142,381.8	221.2	5.401E-10	5.436E-10	0.94
8	12	$2s2p^3\ {}^3P_0^\circ$	142,629	142,393.5	235.5	5.391E-10	5.427E-10	0.94
8	13	$2s2p^3\ {}^1D_2^\circ$	187,422	187,054.0	368	1.828E-10	1.835E-10	0.91
8	14	$2s2p^3\ {}^3S_1^\circ$	197,401	197,087.7	313.3	6.966E-11	7.001E-11	0.93
8	15	$2s2p^3\ {}^1P_1^\circ$	210,920	210,461.8	458.2	9.140E-11	9.212E-11	0.90+0.02 $2s^22p3s\ {}^1P^\circ$
8	16	$2s^22p3s\ {}^3P_0^\circ$	267,120	267,258.71	−138.71	2.539E-10	2.550E-10	0.94+0.03 $2p^3({}^2P)3s\ {}^3P^\circ$
8	17	$2s^22p3s\ {}^3P_1^\circ$	267,233	267,377.11	−144.11	2.537E-10	2.549E-10	0.93+0.03 $2p^3({}^2P)3s\ {}^3P^\circ$
8	18	$2s^22p3s\ {}^3P_2^\circ$	267,491	267,634.00	−143	2.535E-10	2.547E-10	0.94+0.03 $2p^3({}^2P)3s\ {}^3P^\circ$
8	19	$2s^22p3s\ {}^1P_1^\circ$	272,971	273,081.33	−110.33	2.079E-10	2.086E-10	0.92+0.03 $2p^3({}^2P)3s\ {}^1P^\circ$
8	20	$2p^4\ {}^3P_2$	284,208	283,759.70	448.3	1.647E-10	1.663E-10	0.88
8	21	$2p^4\ {}^3P_1$	284,425	283,977.40	447.6	1.644E-10	1.661E-10	0.88
8	22	$2p^4\ {}^3P_0$	284,541	284,071.90	469.1	1.642E-10	1.660E-10	0.88
8	23	$2s^22p3p\ {}^1P_1$	290,832	290,958.25	−126.25	8.136E-09	8.286E-09	0.93+0.03 $2p^3({}^2P)3p\ {}^1P$
8	24	$2s^22p3p\ {}^3D_1$	293,741	293,866.49	−125.49	5.339E-09	5.389E-09	0.94+0.03 $2p^3({}^2P)3p\ {}^3D$
8	25	$2s^22p3p\ {}^3D_2$	293,879	294,002.86	−123.86	5.325E-09	5.376E-09	0.94+0.03 $2p^3({}^2P)3p\ {}^3D$
8	26	$2s^22p3p\ {}^3D_3$	294,103	294,223.07	−120.07	5.311E-09	5.361E-09	0.94+0.03 $2p^3({}^2P)3p\ {}^3D$
8	27	$2s^22p3p\ {}^3S_1$	297,426	297,558.66	−132.66	2.330E-09	2.366E-09	0.94+0.04 $2p^3({}^2P)3p\ {}^3S$
8	28	$2p^4\ {}^1D_2$	298,908	298,294.0	614	4.227E-10	4.258E-10	0.87+0.02 $2p^3({}^2D)3p\ {}^1D$
8	29	$2s^22p3p\ {}^3P_0$	300,128	300,229.93	−101.93	2.888E-09	2.931E-09	0.91+0.03 $2p^3({}^2P)3p\ {}^3P$ + 0.03 $2s2p^2({}^3P)3s\ {}^3P$
8	30	$2s^22p3p\ {}^3P_1$	300,206	300,311.96	−105.96	2.877E-09	2.920E-09	0.91+0.03 $2p^3({}^2P)3p\ {}^3P$ + 0.03 $2s2p^2({}^3P)3s\ {}^3P$
8	31	$2s^22p3p\ {}^3P_2$	300,337	300,442.55	−105.55	2.858E-09	2.904E-09	0.91+0.03 $2p^3({}^2P)3p\ {}^3P$ + 0.03 $2s2p^2({}^3P)3s\ {}^3P$
8	32	$2s^22p3p\ {}^1D_2$	306,543	306,586.08	−43.08	3.316E-09	3.348E-09	0.93+0.03 $2p^3({}^2P)3p\ {}^1D$
8	33	$2s^22p3p\ {}^1S_0$	313,831	313,802.77	28.23	1.637E-09	1.652E-09	0.91+0.03 $2p^3({}^2P)3p^1\ S$
8	34	$2s^22p3d\ {}^3F_2^\circ$	324,423	324,464.88	−41.88	3.213E-10	3.225E-10	0.66+0.28 $2s^22p3d\ {}^1D^\circ$ + 0.02 $2p^3({}^2P)3d^3F^\circ$
8	35	$2s^22p3d\ {}^3F_3^\circ$	324,634	324,660.80	−26.8	4.134E-09	4.153E-09	0.94+0.03 $2p^3({}^2P)3d^3F^\circ$
8	36	$2s^22p3d\ {}^1D_2^\circ$	324,694	324,735.65	−41.65	1.405E-10	1.410E-10	0.66+0.28 $2s^22p3d\ {}^3F^\circ$ + 0.02 $2p^3({}^2P)3d\ {}^1D^\circ$
8	37	$2s^22p3d\ {}^3F_4^\circ$	324,825	324,839.03	−14.03	5.144E-09	5.168E-09	0.94+0.04 $2p^3({}^2P)3d\ {}^3F^\circ$
8	38	$2s^22p3d\ {}^3D_1^\circ$	327,167	327,229.25	−62.25	4.890E-11	4.898E-11	0.94+0.03 $2p^3({}^2P)3d\ {}^3D^\circ$
8	39	$2s^22p3d\ {}^3D_2^\circ$	327,220	327,278.30	−58.3	4.902E-11	4.910E-11	0.94+0.03 $2p^3({}^2P)3d\ {}^3D^\circ$
8	40	$2s^22p3d\ {}^3D_3^\circ$	327,300	327,352.17	−52.17	4.898E-11	4.905E-11	0.94+0.03 $2p^3({}^2P)3d\ {}^3D^\circ$
8	41	$2s^22p3d\ {}^3P_2^\circ$	329,409	329,469.80	−60.8	8.363E-11	8.384E-11	0.93+0.04 $2p^3({}^2P)3d\ {}^3P^\circ$
8	42	$2s^22p3d\ {}^3P_1^\circ$	329,517	329,583.89	−66.89	8.362E-11	8.383E-11	0.94+0.04 $2p^3({}^2P)3d\ {}^3P^\circ$
8	43	$2s^22p3d\ {}^3P_0^\circ$	329,582	329,645.14	−63.14	8.373E-11	8.394E-11	0.94+0.04 $2p^3({}^2P)3d\ {}^3P^\circ$
8	44	$2s^22p3d\ {}^1F_3^\circ$	331,825	331,821.44	3.56	5.044E-11	5.046E-11	0.94+0.04 $2p^3({}^2P)3d\ {}^1F^\circ$
8	45	$2s^22p3d\ {}^1P_1^\circ$	332,748	332,778.94	−30.94	8.047E-11	8.058E-11	0.93+0.04 $2p^3({}^2P)3d\ {}^1P^\circ$
8	46	$2s2p^2({}^3P)3s\ {}^5P_1$	338,427	338,577.25	−150.25	3.086E-10	3.098E-10	0.99
8	47	$2s2p^2({}^3P)3s\ {}^5P_2$	338,551	338,701.98	−150.98	3.083E-10	3.095E-10	0.99
8	48	$2s2p^2({}^3P)3s\ {}^5P_3$	338,716	338,863.03	−147.03	3.079E-10	3.091E-10	0.99
8	49	$2p^4\ {}^1S_0$	344,147	343,306.3	840.7	1.658E-10	1.694E-10	0.81+0.05 $2s^22p^2\ {}^1S$ + 0.03 $2p^3({}^2P)3p^1\ S$
8	50	$2s2p^2({}^3P)3s\ {}^3P_0$	349,990	350,024.49	−34.49	2.368E-10	2.380E-10	0.87+0.07 $2s^22p4p\ {}^3P$ + 0.02 $2s^22p3p\ {}^3P$
8	51	$2s2p^2({}^3P)3s\ {}^3P_1$	350,088	350,124.45	−36.45	2.366E-10	2.378E-10	0.87+0.07 $2s^22p4p\ {}^3P$ + 0.02 $2s^22p3p\ {}^3P$
8	52	$2s2p^2({}^3P)3s\ {}^3P_2$	350,261	350,298.38	−37.38	2.363E-10	2.375E-10	0.87+0.07 $2s^22p4p\ {}^3P$ + 0.02 $2s^22p3p\ {}^3P$
8	53	$2s^22p4s\ {}^3P_0^\circ$	356,640	356,736.30	−96.3	5.330E-10	5.365E-10	0.94+0.04 $2p^3({}^2P)4s\ {}^3P^\circ$
8	54	$2s^22p4s\ {}^3P_1^\circ$	356,744	356,844.98	−100.98	5.289E-10	5.324E-10	0.93+0.03 $2p^3({}^2P)4s\ {}^3P^\circ$
8	55	$2s^22p4s\ {}^3P_2^\circ$	357,016	357,117.01	−101.01	5.306E-10	5.341E-10	0.93+0.04 $2p^3({}^2P)4s\ {}^3P^\circ$
8	56	$2s^22p4s\ {}^1P_1^\circ$	358,634	358,668.90	−34.9	3.177E-10	3.205E-10	0.93+0.03 $2p^3({}^2P)4s\ {}^1P^\circ$
8	57	$2s2p^2({}^3P)3p\ {}^3S_1^\circ$	363,163	363,263.38	−100.38	2.560E-10	2.574E-10	0.96
8	58	$2s2p^2({}^3P)3p\ {}^5D_0^\circ$	365,416	365,527.08	−111.08	9.095E-09	9.118E-09	0.99
8	59	$2s2p^2({}^3P)3p\ {}^5D_1^\circ$	365,449	365,561.95	−112.95	9.094E-09	9.126E-09	0.99
8	60	$2s2p^2({}^3P)3p\ {}^5D_2^\circ$	365,518	365,630.40	−112.4	9.092E-09	9.125E-09	0.99
8	61	$2s^22p4p\ {}^1P_1$	365,598	365,726.76	−128.76	1.709E-09	1.723E-09	0.91+0.03 $2p^3({}^2P)4p\ {}^1P$ + 0.02 $2s^22p4p\ {}^3D$
8	62	$2s2p^2({}^3P)3p\ {}^5D_3^\circ$	365,622	365,730.68	−108.68	9.078E-09	9.093E-09	0.99
8	63	$2s2p^2({}^3P)3p\ {}^5D_4^\circ$	365,754	365,857.89	−103.89	9.059E-09	9.053E-09	0.99

Table 2
(Continued)

Z	Key	Level	E_{MCDHF}	E_{NIST}	ΔE	$\tau^{l}_{\mathrm{MCDHF}}$	$\tau^{v}_{\mathrm{MCDHF}}$	LS Composition
8	64	$2s^22p4p\ ^3D_1$	366,377	366,488.45	−111.45	1.952E-09	1.945E-09	$0.91+0.03\ 2p^3(^2P)4p\ ^3D + 0.02\ 2s^22p4p\ \ ^1P$
8	65	$2s^22p4p\ ^3D_2$	366,485	366,595.76	−110.76	1.959E-09	1.951E-09	$0.93+0.03\ 2p^3(^2P)4p\ ^3D$
8	66	$2s^22p4p\ ^3D_3$	366,694	366,802.62	−108.62	1.955E-09	1.947E-09	$0.93+0.03\ 2p^3(^2P)4p\ ^3D$
8	67	$2s^22p4p\ ^3S_1$	367,869	367,953.90	−84.9	1.878E-09	1.917E-09	$0.94+0.04\ 2p^3(^2P)4p\ ^3S$
8	68	$2s2p^2(^3P)3p\ ^5P_1°$	368,415	368,538.65	−123.65	6.914E-09	6.925E-09	0.99
8	69	$2s2p^2(^3P)3p\ ^5P_2°$	368,472	368,595.93	−123.93	6.935E-09	6.951E-09	0.99
8	70	$2s2p^2(^3P)3p\ ^5P_3°$	368,576	368,697.00	−121	6.906E-09	6.909E-09	0.99
8	71	$2s^22p4p\ ^3P_0$	370,426	370,329.18	96.82	2.626E-09	2.592E-09	$0.87+0.06\ 2s2p^2(^3P)3s\ ^3P + 0.03\ 2p^3(^2P)4p\ ^3P$
8	72	$2s^22p4p\ ^3P_1$	370,510	370,418.32	91.68	2.619E-09	2.584E-09	$0.87+0.06\ 2s2p^2(^3P)3s\ ^3P + 0.03\ 2p^3(^2P)4p\ ^3P$
8	73	$2s^22p4p\ ^3P_2$	370,619	370,526.49	92.51	2.637E-09	2.605E-09	$0.83+0.06\ 2s2p^2(^3P)3s\ ^3P + 0.04\ 2s^22p4p\ \ ^1D$
8	74	$2s^22p4p\ ^1D_2$	371,012	370,902.22	109.78	3.219E-09	3.277E-09	$0.88+0.04\ 2s^22p4p\ \ ^3P + 0.03\ 2p^3(^2P)4p\ ^1D$
8	75	$2s^22p4p\ ^1S_0$	374,237			3.008E-09	3.110E-09	$0.90+0.03\ 2p^3(^2P)4p^1S + 0.03\ 2s^22p5p\ \ ^1S$
8	76	$2s2p^2(^3P)3p\ ^3D_1°$	374,531	374,571.64	−40.64	1.285E-10	1.291E-10	$0.87+0.08\ 2s^22p4d\ \ ^3D° + 0.02\ 2s2p^2(^1D)3p\ ^3D°$
8	77	$2s2p^2(^3P)3p\ ^3D_2°$	374,622	374,663.52	−41.52	1.278E-10	1.284E-10	$0.87+0.08\ 2s^22p4d\ \ ^3D° + 0.02\ 2s2p^2(^1D)3p\ ^3D°$
8	78	$2s2p^2(^3P)3p\ ^3D_3°$	374,757	374,795.14	−38.14	1.269E-10	1.275E-10	$0.87+0.08\ 2s^22p4d\ \ ^3D°$
8	79	$2s2p^2(^3P)3p\ ^5S_2°$	376,016	376,079.92	−63.92	3.076E-09	3.114E-09	0.97
8	80	$2s^22p4d\ ^3F_2°$	377,259	377,385.58	−126.58	8.337E-10	8.383E-10	$0.76+0.18\ 2s^22p4d\ \ ^1D° + 0.03\ 2p^3(^2P)4d\ ^3F°$
8	81	$2s^22p4d\ ^3F_3°$	377,440	377,562.31	−122.31	2.494E-09	2.478E-09	$0.94+0.04\ 2p^3(^2P)4d\ ^3F°$
8	82	$2s^22p4d\ ^1D_2°$	377,562	377,686.83	−124.83	2.635E-10	2.660E-10	$0.74+0.18\ 2s^22p4d\ \ ^3F° + 0.03\ 2p^3(^2P)4d\ ^1D°$
8	83	$2s^22p4d\ ^3F_4°$	377,630	377,748.57	−118.57	2.718E-09	2.697E-09	$0.95+0.04\ 2p^3(^2P)4d\ ^3F°$
8	84	$2s^22p4d\ ^3P_2°$	378,320	378,405.68	−85.68	1.194E-10	1.198E-10	$0.52+0.41\ 2s2p^2(^3P)3p\ ^3P° + 0.02\ 2p^3(^2P)4d\ ^3P°$
8	85	$2s^22p4d\ ^3P_1°$	378,337	378,417.84	−80.84	1.193E-10	1.197E-10	$0.49+0.45\ 2s2p^2(^3P)3p\ ^3P°$
8	86	$2s2p^2(^3P)3p\ ^3P_0°$	378,362	378,435.16	−73.16	1.195E-10	1.199E-10	$0.48+0.48\ 2s^22p4d\ \ ^3P°$
8	87	$2s^22p4d\ ^3D_1°$	379,128	379,227.15	−99.15	1.811E-10	1.821E-10	$0.86+0.08\ 2s2p^2(^3P)3p\ ^3D° + 0.03\ 2p^3(^2P)4d\ ^3D°$
8	88	$2s^22p4d\ ^3D_2°$	379,195	379,293.03	−98.03	1.822E-10	1.832E-10	$0.85+0.08\ 2s2p^2(^3P)3p\ ^3D° + 0.03\ 2p^3(^2P)4d\ ^3D°$
8	89	$2s^22p4d\ ^3D_3°$	379,261	379,356.75	−95.75	1.845E-10	1.856E-10	$0.86+0.08\ 2s2p^2(^3P)3p\ ^3D° + 0.03\ 2p^3(^2P)4d\ ^3D°$
8	90	$2s^22p4f\ ^3F_2$	380,530	380,621.90	−91.9	7.816E-10	7.839E-10	$0.90+0.03\ 2p^3(^2P)4f\ ^3F + 0.03\ 2s^22p4f\ \ ^1D$
8	91	$2s^22p4f\ ^1F_3$	380,532	380,612.20	−80.2	7.806E-10	7.832E-10	$0.60+0.30\ 2s^22p4f\ \ ^3F + 0.05\ 2s^22p4f\ \ ^3D$
8	92	$2s^22p4f\ ^3F_3$	380,578	380,671.30	−93.3	7.807E-10	7.825E-10	$0.58+0.27\ 2s^22p4f\ \ ^1F + 0.11\ 2s^22p4f\ \ ^3G$
8	93	$2s^22p4f\ ^3F_4$	380,610	380,685.90	−75.9	7.836E-10	7.869E-10	$0.85+0.06\ 2s^22p4f\ \ ^3G + 0.04\ 2s^22p4f\ \ ^1G$
8	94	$2s2p^2(^3P)3p\ ^3P_2°$	380,704	380,706.51	−2.51	2.712E-09	2.752E-09	$0.51+0.41\ 2s^22p4d\ \ ^3P°$
8	95	$2s2p^2(^3P)3p\ ^3P_1°$	380,709	380,717.92	−8.92	1.757E-09	1.780E-09	$0.46+0.44\ 2s^22p4d\ \ ^3P° + 0.02\ 2s^22p4d\ \ ^1P°$
8	96	$2s^22p4d\ ^3P_0°$	380,732	380,737.00	−5	2.159E-09	2.195E-09	$0.47+0.45\ 2s2p^2(^3P)3p\ ^3P°$
8	97	$2s^22p4d\ ^1F_3°$	380,746	380,782.17	−36.17	9.777E-11	9.814E-11	$0.94+0.04\ 2p^3(^2P)4d\ ^1F°$
8	98	$2s^22p4d\ ^1P_1°$	381,057	381,089.27	−32.27	1.608E-10	1.617E-10	$0.91+0.04\ 2p^3(^2P)4d\ ^1P°$
8	99	$2s^22p4f\ ^3G_3$	381,092	381,176.90	−84.9	7.995E-10	7.995E-10	$0.84+0.06\ 2s^22p4f\ \ ^1F + 0.05\ 2s^22p4f\ \ ^3F$
8	100	$2s^22p4f\ ^3G_4$	381,142	381,211.30	−69.3	8.170E-10	8.186E-10	$0.66+0.20\ 2s^22p4f\ \ ^1G + 0.10\ 2s^22p4f\ \ ^3F$
8	101	$2s^22p4f\ ^3G_5$	381,339	381,404.50	−65.5	8.027E-10	8.031E-10	$0.95+0.04\ 2p^3(^2P)4f^3G$
8	102	$2s^22p4f\ ^3D_3$	381,365	381,456.80	−91.8	8.178E-10	8.189E-10	$0.90+0.03\ 2p^3(^2P)4f^3\ D + 0.03\ 2s^22p4f\ \ ^3F$
8	103	$2s^22p4f\ ^3D_2$	381,375	381,477.80	−102.8	8.427E-10	8.439E-10	$0.49+0.41\ 2s^22p4f\ \ ^1D + 0.05\ 2s^22p4f\ \ ^3F$
8	104	$2s^22p4f\ ^1G_4$	381,393	381,472.50	−79.5	8.698E-10	8.732E-10	$0.72+0.23\ 2s^22p4f\ \ ^3G + 0.03\ 2p^3(^2P)4f\ ^1G$
8	105	$2s^22p4f\ ^3D_1$	381,522	381,623.80	−101.8	8.206E-10	8.210E-10	$0.95+0.04\ 2p^3(^2P)4f\ ^3D$
8	106	$2s^22p4f\ ^1D_2$	381,557	381,645.00	−88	8.515E-10	8.535E-10	$0.51+0.44\ 2s^22p4f\ \ ^3D$
8	107	$2s^22p5s\ ^3P_0°$	391,736	391,830.76	−94.76	6.995E-10	7.161E-10	$0.93+0.03\ 2p^3(^2P)5s\ ^3P°$
8	108	$2s^22p5s\ ^3P_1°$	391,821	391,917.80	−96.8	6.874E-10	7.042E-10	$0.90+0.04\ 2s^22p5s\ \ ^1P° +0.03\ 2p^3(^2P)5s\ ^3P°$
8	109	$2s^22p5s\ ^3P_2°$	392,110	392,209.53	−99.53	6.947E-10	7.115E-10	$0.94+0.04\ 2p^3(^2P)5s\ ^3P°$
8	110	$2s^22p5s\ ^1P_1°$	392,753	392,781.47	−28.47	5.117E-10	5.305E-10	$0.91+0.04\ 2s^22p5s\ \ ^3P° + 0.03\ 2p^3(^2P)5s\ ^1P°$
8	111	$2s2p^2(^1D)3s\ ^3D_1$	394,069	394,079.4	−10.4	2.427E-10	2.428E-10	$0.54+0.40\ 2s^22p5p\ \ ^3D$
8	112	$2s2p^2(^1D)3s\ ^3D_2$	394,123	394,127.3	−4.3	2.368E-10	2.369E-10	$0.55+0.39\ 2s^22p5p\ \ ^3D$
8	113	$2s2p^2(^1D)3s\ ^3D_3$	394,209	394,197.9	11.1	2.288E-10	2.290E-10	$0.58+0.37\ 2s^22p5p\ \ ^3D$
8	114	$2s2p^2(^3P)3d\ ^5F_1$	394,462	394,528.20	−66.2	5.948E-09	5.924E-09	0.99
8	115	$2s2p^2(^3P)3d\ ^5F_2$	394,503	394,567.05	−64.05	5.943E-09	5.920E-09	0.99
8	116	$2s2p^2(^3P)3d\ ^5F_3$	394,567	394,624.68	−57.68	5.940E-09	5.911E-09	0.99
8	117	$2s2p^2(^3P)3d\ ^5F_4$	394,654	394,700.27	−46.27	5.946E-09	5.907E-09	0.99
8	118	$2s2p^2(^3P)3d\ ^5F_5$	394,757	394,793.28	−36.28	5.960E-09	5.913E-09	0.99
8	119	$2s^22p5p\ ^1P_1$	395,976			1.911E-09	2.020E-09	$0.93+0.03\ 2p^3(^2P)5p\ ^1P$
8	120	$2s^22p5p\ ^3S_1$	397,054			2.073E-09	2.242E-09	$0.91+0.04\ 2p^3(^2P)5p\ ^3S$
8	121	$2s^22p5p\ ^1D_2$	397,904			1.317E-09	1.340E-09	$0.58+0.18\ 2s^22p5p\ \ ^3P + 0.09\ 2s2p^2(^1D)3s\ ^1D$
8	122	$2s^22p5p\ ^3P_0$	397,909			3.232E-09	3.234E-09	$0.93+0.04\ 2p^3(^2P)5p\ ^3P$
8	123	$2s^22p5p\ ^3P_1$	397,990			2.127E-09	2.142E-09	$0.86+0.03\ 2p^3(^2P)5p^3P + 0.03\ 2s^22p5p\ \ ^3D$
8	124	$2s2p^2(^3P)3d\ ^5D_2$	398,038	398,139.92	−101.92	6.260E-10	6.271E-10	$0.93+0.06\ 2s2p^2(^3P)3d\ ^5P$
8	125	$2s2p^2(^3P)3d\ ^5D_1$	398,039	398,144.29	−105.29	1.472E-09	1.475E-09	$0.97+0.02\ 2s2p^2(^3P)3d\ ^5P$
8	126	$2s2p^2(^3P)3d\ ^5D_0$	398,045	398,145.63	−100.63	4.776E-09	4.788E-09	0.99
8	127	$2s2p^2(^3P)3d\ ^5D_3$	398,052	398,150.40	−98.4	3.442E-10	3.448E-10	$0.87+0.12\ 2s2p^2(^3P)3d\ ^5P$

Table 2
(Continued)

Z	Key	Level	$E_{\rm MCDHF}$	$E_{\rm NIST}$	ΔE	$\tau^{l}_{\rm MCDHF}$	$\tau^{v}_{\rm MCDHF}$	LS Composition
8	128	$2s2p^2(^3P)3d\ ^5D_4$	398,140	398,231.48	−91.48	4.878E-09	4.885E-09	0.99
8	129	$2s^22p5p\ ^3P_2$	398,144			2.387E-09	2.415E-09	0.69+0.20 $2s^22p5p\ ^1D$ +0.03 $2s2p^2(^1D)3s\ ^1D$
8	130	$2s^22p5p\ ^3D_1$	398,278			3.789E-10	3.841E-10	0.52+0.38 $2s2p^2(^1D)3s\ ^3D$ + 0.05 $2s^22p5p\ ^3P$
8	131	$2s^22p5p\ ^3D_2$	398,378			3.895E-10	3.946E-10	0.51+0.34 $2s2p^2(^1D)3s\ ^3D$ + 0.05 $2s^22p5p\ ^3P$
8	132	$2s2p^2(^3P)3d\ ^5P_3$	398,382	398,487.08	−105.08	5.166E-11	5.174E-11	0.85+0.12 $2s2p^2(^3P)3d\ ^5D$
8	133	$2s2p^2(^3P)3d\ ^5P_2$	398,450	398,557.17	−107.17	4.797E-11	4.804E-11	0.91+0.06 $2s2p^2(^3P)3d\ ^5D$
8	134	$2s^22p5p\ ^3D_3$	398,457			3.458E-10	3.500E-10	0.57+0.36 $2s2p^2(^1D)3s\ ^3D$ + 0.02 $2p^3(^2P)5p\ ^3D$
8	135	$2s2p^2(^3P)3d\ ^5P_1$	398,486	398,595.65	−109.65	4.561E-11	4.567E-11	0.96+0.02 $2s2p^2(^3P)3d\ ^5D$
8	136	$2s2p^2(^3P)3d\ ^3P_2$	400,289	400,351.56	−62.56	1.159E-10	1.162E-10	0.96
8	137	$2s2p^2(^3P)3d\ ^3P_1$	400,402	400,460.99	−58.99	1.157E-10	1.161E-10	0.96
8	138	$2s2p^2(^3P)3d\ ^3P_0$	400,466	400,514.89	−48.89	1.156E-10	1.160E-10	0.96
8	139	$2s^22p5p\ ^1S_0$	401,102			2.667E-09	3.060E-09	0.90+0.03 $2p^3(^2P)5p\ ^1S$
8	140	$2s2p^2(^3P)3d\ ^3F_2$	401,349	401,375.09	−26.09	1.084E-10	1.083E-10	0.98
8	141	$2s^22p5d\ ^3F_2^\circ$	401,386	401,519.8	−133.8	1.231E-09	1.279E-09	0.74+0.21 $2s^22p5d\ ^1D^\circ$ + 0.03 $2p^3(^2P)5d\ ^3F^\circ$
8	142	$2s2p^2(^3P)3d\ ^3F_3$	401,448	401,476.29	−28.29	1.083E-10	1.082E-10	0.98
8	143	$2s^22p5d\ ^3F_3^\circ$	401,557	401,725.6	−168.6	2.157E-09	2.217E-09	0.92+0.03 $2p^3(^2P)5d\ ^3F^\circ$ + 0.02 $2s^22p5d\ ^3D^\circ$
8	144	$2s2p^2(^3P)3d\ ^3F_4$	401,578	401,605.52	−27.52	1.080E-10	1.078E-10	0.98
8	145	$2s^22p5d\ ^1D_2^\circ$	401,659	401,791.7	−132.7	4.662E-10	4.879E-10	0.70+0.20 $2s^22p5d\ ^3F^\circ$ + 0.03 $2p^3(^2P)5d\ ^1D^\circ$
8	146	$2s^22p5d\ ^3F_4^\circ$	401,763	401,893.2	−130.2	3.332E-09	3.395E-09	0.95+0.04 $2p^3(^2P)5d\ ^3F^\circ$
8	147	$2s^22p5d\ ^3D_1^\circ$	402,229			2.086E-10	2.178E-10	0.87+0.06 $2s^22p5d\ ^3P^\circ$ + 0.03 $2p^3(^2P)5d\ ^3D^\circ$
8	148	$2s^22p5d\ ^3D_2^\circ$	402,283	402,411.5	−128.5	2.242E-10	2.338E-10	0.76+0.15 $2s^22p5d\ ^3P^\circ$ +0.03 $2p^3(^2P)5d\ ^3D^\circ$
8	149	$2s^22p5d\ ^3D_3^\circ$	402,401	402,533.3	−132.3	2.071E-10	2.160E-10	0.92+0.03 $2p^3(^2P)5d\ ^3D^\circ$ + 0.02 $2s^22p5d\ ^3F^\circ$
8	150	$2s^22p5d\ ^3P_2^\circ$	402,642			3.065E-10	3.191E-10	0.78+0.17 $2s^22p5d\ ^3D^\circ$ + 0.03 $2p^3(^2P)5d\ ^3P^\circ$
8	151	$2s^22p5d\ ^3P_1^\circ$	402,715			3.257E-10	3.393E-10	0.88+0.07 $2s^22p5d\ ^3D^\circ$ + 0.03 $2p^3(^2P)5d\ ^3P^\circ$
8	152	$2s^22p5d\ ^3P_0^\circ$	402,757			3.417E-10	3.559E-10	0.95+0.04 $2p^3(^2P)5d\ ^3P^\circ$
8	153	$2s^22p5f\ ^1F_3$	403,077			1.536E-09	1.520E-09	0.64+0.12 $2s^22p5f\ ^3D$ +0.12 $2s^22p5f\ ^3F$
8	154	$2s^22p5f\ ^3F_2$	403,086			1.632E-09	1.644E-09	0.79+0.09 $2s^22p5f\ ^1D$ + 0.06 $2s^22p5f\ ^3D$
8	155	$2s^22p5f\ ^3F_3$	403,105			1.590E-09	1.586E-09	0.58+0.28 $2s^22p5f\ ^3G$ + 0.05 $2s^22p5f\ ^1F$
8	156	$2s^22p5f\ ^3F_4$	403,136			1.617E-09	1.626E-09	0.62+0.21 $2s^22p5f\ ^3G$ + 0.12 $2s^22p5f\ ^1G$

Note. $E_{\rm MCDHF}$: the present MCDHF excitation energies; $E_{\rm NIST}$: the compiled values from the NIST database (Kramida et al. 2020); ΔE: energy differences (in cm^{-1}) between $E_{\rm MCDHF}$ the values of and $E_{\rm NIST}$. $\tau^{l}_{\rm MCDHF}$: the present MCDHF lifetimes in length form; $\tau^{v}_{\rm MCDHF}$: the present MCDHF lifetimes in velocity form; LS composition: the LS eigenvector compositions. The results of O III are shown here for guidance regarding its form and content.

(This table is available in its entirety in machine-readable form.)

#15). The average difference with the standard deviation with the compiled values from the NIST database for these higher states are -49 ± 140 cm^{-1} for MCDHF, 722 ± 185 cm^{-1} for MCHF, 5 ± 855 cm^{-1} for MCHF1, and -1377 ± 1376cm^{-1} for AUTOSTRUCTURE. The accuracy of the present MCDHF calculations is far better than those of three previous calculations (MCHF, MCHF1, and AUTOSTRUCTURE) involving higher states. The physical reason is that limited electron correlations were included in the previous calculations. For example, only core–valence and core–core electron correlations from the $2s$ and $2p$ orbitals to the $3l$ and $4l$ ($l = 0$–3) correlated orbitals were considered in the MCHF1 calculations by Tayal & Zatsarinny (2017). By comparison, core–valence and core–core electron correlations from the $2s$ and $2p$ orbitals to the nl ($n \leqslant 10$ and $l \leqslant 6$) correlated orbitals, as well as core–valence electron correlation from the $1s$ orbital to the nl ($n \leqslant 10$ and $l \leqslant 6$) correlated orbitals, are included in the present MCDHF calculations. A complete data set of the 156 lowest states of the $n \leqslant 5$ configurations is provided by our MCDHF calculations.

Excitation energies $E_{\rm NIST}$ are available in the NIST database for many states along the C-like isoelectronic sequence from O III to Mg VII. All these NIST values are included in Table 2. To further evaluate the accuracy of our MCDHF excitation energies $E_{\rm MCDHF}$, the energy differences $\Delta E = E_{\rm MCDHF} - E_{\rm NIST}$ are also provided in this table. It is clearly shown that the differences ΔE are generally about 100 cm^{-1}–200 cm^{-1} or smaller. More specifically, excluding 26 states for which the differences ΔE are greater than 900 cm^{-1} (they will be discussed in the following), the average difference with a standard deviation of the NIST and MCDHF excitation energies in C-like ions from O III to Mg VII is -1 ± 184 cm^{-1}.

There are 26 states in Table 2, including three states in F IV, one state in Ne V, 16 states in Na VI, and six states in Mg VII, for which the differences $\Delta E = E_{\rm MCDHF} - E_{\rm NIST}$ are larger than 900 cm^{-1}. As an example, the energy differences $\Delta E = E_{\rm MCDHF} - E_{\rm NIST}$ for the states $2s^2\,2p\,3p\ ^1D_2$, $2s\,2p^2(^3P)3d\ ^5D_2$, $2s\,2p^2(^3P)3d\ ^5D_3$, $2s^2\,2p\,4s\ ^3P_2^\circ$, and $2s^2\,2p\,4d\ ^3F_2^\circ$ are displayed in Figure 1 as functions of the nuclear charge Z. Anomalies appear for five states in Na VI, whereas energy differences ΔE are within 200 cm^{-1} for all the other states along the electronic sequence. The present MCDHF calculations apply the same computational procedures for all ions in the isoelectronic sequence, and the differences with the compiled values from the NIST database along the sequence are thus expected to be smooth. This is not the case, which indicates that the identifications involving these five states in Na VI are questionable, or that the accuracy of observed wavelengths for these five states is low. Using spectral lines of Na VI, we further discuss this issue in Section 3.2.

Table 3

Transition Wavelengths λ (in Å), Transition Rates A (in s^{-1}), Weighted Oscillator Strengths gf, and Line Strengths S (in au) between the States of O III (F IV, Ne V, Na VI, Mg VII) Listed in Table 2

Z	i	j	λ	Type	BF	$A_l(AS_5)$	$A_l(AS_4)$	$A_v(AS_5)$	$gf_l(AS_5)$	$gf_l(AS_4)$	$gf_v(AS_5)$	$S_l(AS_5)$	$S_l(AS_4)$	$S_v(AS_5)$	Acc.
11	1	2	1.44281E+05	M1	1.000E+00	5.980E-03	5.964E-03		5.599E-08	5.594E-08		1.998E+00	1.998E+00		AA
11	1	4	2.80988E+03	E2	3.654E-05	5.868E-05	5.862E-05	4.779E-05	3.473E-13	3.466E-13	2.828E-13	4.589E-05	4.574E-05	3.737E-05	B+
11	1	9	4.89320E+02	E1	5.827E-01	8.385E+08	8.380E+08	8.366E+08	9.030E-02	9.028E-02	9.009E-02	1.455E-01	1.455E-01	1.451E-01	A
11	1	11	4.14034E+02	E1	3.274E-01	1.251E+09	1.251E+09	1.249E+09	9.646E-02	9.646E-02	9.627E-02	1.315E-01	1.315E-01	1.312E-01	A
11	1	14	3.11728E+02	E1	1.106E-01	2.785E+09	2.784E+09	2.778E+09	1.217E-01	1.217E-01	1.214E-01	1.249E-01	1.249E-01	1.246E-01	A
11	1	22	1.23893E+02	E1	3.299E-01	1.061E+10	1.060E+10	1.059E+10	7.323E-02	7.321E-02	7.314E-02	2.987E-02	2.986E-02	2.983E-02	A
11	1	24	1.22304E+02	E1	1.042E-03	5.186E+07	5.172E+07	5.164E+07	3.489E-04	3.480E-04	3.474E-04	1.405E-04	1.401E-04	1.399E-04	B+
11	1	27	1.16240E+02	E2	1.129E-03	1.204E+06	1.204E+06	1.203E+06	1.220E-05	1.219E-05	1.218E-05	1.141E-01	1.141E-01	1.140E-01	B+
11	1	32	1.14518E+02	E2	7.452E-05	3.298E+05	3.298E+05	3.293E+05	3.242E-06	3.243E-06	3.237E-06	2.900E-02	2.901E-02	2.896E-02	B+
11	1	42	1.07563E+02	E1	6.388E-01	1.607E+11	1.607E+11	1.607E+11	8.364E-01	8.364E-01	8.363E-01	2.962E-01	2.962E-01	2.961E-01	A
11	1	46	1.07022E+02	E1	1.880E-01	2.743E+10	2.744E+10	2.741E+10	1.413E-01	1.414E-01	1.412E-01	4.978E-02	4.982E-02	4.975E-02	A
11	1	49	1.05647E+02	E1	1.828E-03	3.223E+08	3.240E+08	3.218E+08	1.618E-03	1.626E-03	1.616E-03	5.628E-04	5.657E-04	5.619E-04	B+
11	1	53	1.03024E+02	E1	1.179E-01	6.896E+09	6.892E+09	6.893E+09	3.292E-02	3.291E-02	3.291E-02	1.116E-02	1.116E-02	1.116E-02	A
11	1	55	1.02457E+02	E1	1.571E-03	4.787E+05	4.797E+05	4.730E+05	2.260E-06	2.265E-06	2.233E-06	7.623E-07	7.642E-07	7.533E-07	B
11	1	59	1.01814E+02	E1	5.063E-02	2.489E+07	2.484E+07	2.490E+07	1.160E-04	1.158E-04	1.161E-04	3.890E-05	3.883E-05	3.890E-05	B+
11	1	62	1.00465E+02	E1	5.760E-01	2.759E+10	2.759E+10	2.760E+10	1.253E-01	1.253E-01	1.253E-01	4.143E-02	4.143E-02	4.144E-02	A
11	1	67	9.94732E+01	E1	2.842E-01	1.302E+10	1.303E+10	1.304E+10	5.796E-02	5.802E-02	5.802E-02	1.898E-02	1.900E-02	1.900E-02	A
11	1	86	9.54741E+01	E2	3.417E-05	3.173E+06	3.172E+06	3.172E+06	2.168E-05	2.168E-05	2.167E-05	1.124E-01	1.124E-01	1.123E-01	B+
11	1	89	9.48853E+01	E2	6.878E-05	7.062E+06	7.064E+06	7.060E+06	4.766E-05	4.768E-05	4.765E-05	2.425E-01	2.426E-01	2.424E-01	B+
11	1	93	9.36365E+01	E2	3.314E-05	4.386E+06	4.390E+06	4.388E+06	2.883E-05	2.886E-05	2.884E-05	1.410E-01	1.411E-01	1.410E-01	B+
11	1	101	9.26954E+01	E1	2.438E-01	1.466E+09	1.474E+09	1.470E+09	5.666E-03	5.696E-03	5.681E-03	1.729E-03	1.738E-03	1.734E-03	B+
11	1	105	9.25728E+01	E1	1.362E-01	2.202E+09	2.188E+09	2.188E+09	8.486E-03	8.433E-03	8.433E-03	2.586E-03	2.570E-03	2.570E-03	B+
11	1	107	9.24027E+01	E1	4.318E-04	4.034E+07	4.029E+07	3.998E+07	1.549E-04	1.547E-04	1.535E-04	4.712E-05	4.708E-05	4.670E-05	B+
11	1	109	9.16202E+01	E1	8.026E-03	1.152E+08	1.149E+08	1.154E+08	4.349E-04	4.337E-04	4.359E-04	1.312E-04	1.308E-04	1.315E-04	B+
11	1	113	9.13555E+01	E1	2.303E-01	3.736E+09	3.747E+09	3.736E+09	1.403E-02	1.407E-02	1.402E-02	4.218E-03	4.230E-03	4.217E-03	B+
11	1	118	9.01931E+01	E2	9.448E-05	6.698E+05	6.702E+05	6.640E+05	4.084E-06	4.087E-06	4.049E-06	1.785E-02	1.786E-02	1.769E-02	B+
11	1	124	8.96702E+01	E2	2.692E-05	1.220E+05	1.228E+05	1.211E+05	7.353E-07	7.400E-07	7.297E-07	3.158E-03	3.178E-03	3.134E-03	B+
11	1	138	8.82230E+01	E1	5.986E-01	6.285E+10	6.295E+10	6.281E+10	2.200E-01	2.204E-01	2.199E-01	6.391E-02	6.401E-02	6.386E-02	A
11	1	145	8.81159E+01	E1	1.386E-01	3.483E+09	3.381E+09	3.482E+09	1.216E-02	1.181E-02	1.216E-02	3.528E-03	3.425E-03	3.528E-03	B+
11	1	148	8.80186E+01	E1	1.320E-02	1.570E+09	1.589E+09	1.568E+09	5.471E-03	5.536E-03	5.465E-03	1.585E-03	1.604E-03	1.584E-03	B+
11	1	151	8.79845E+01	E1	1.272E-01	7.741E+09	7.773E+09	7.729E+09	2.695E-02	2.707E-02	2.691E-02	7.807E-03	7.840E-03	7.795E-03	B+
11	1	153	8.77321E+01	E2	1.614E-04	4.242E+06	4.231E+06	4.247E+06	2.447E-05	2.441E-05	2.451E-05	9.843E-02	9.818E-02	9.856E-02	B+
11	1	160	8.75332E+01	E2	3.895E-05	8.662E+05	8.644E+05	8.669E+05	4.975E-06	4.965E-06	4.979E-06	1.987E-02	1.983E-02	1.989E-02	B+
11	1	161	8.75181E+01	E1	6.103E-02	1.153E+09	1.152E+09	1.152E+09	3.971E-03	3.969E-03	3.970E-03	1.144E-03	1.144E-03	1.144E-03	B+
11	1	166	8.72517E+01	E1	2.179E-01	2.782E+09	2.749E+09	2.789E+09	9.526E-03	9.414E-03	9.551E-03	2.736E-03	2.704E-03	2.743E-03	B+
11	1	177	8.67518E+01	E1	1.849E-01	4.660E+09	4.646E+09	4.659E+09	1.577E-02	1.573E-02	1.577E-02	4.504E-03	4.491E-03	4.504E-03	B+
11	1	179	8.63297E+01	E1	4.449E-02	2.270E+09	2.268E+09	2.275E+09	7.608E-03	7.603E-03	7.625E-03	2.162E-03	2.161E-03	2.167E-03	B+
11	1	187	8.33975E+01	E2	4.914E-05	1.581E+06	1.551E+06	1.582E+06	8.244E-06	8.084E-06	8.247E-06	2.848E-02	2.793E-02	2.849E-02	B+
11	1	188	8.32249E+01	E2	1.118E-04	5.489E+06	5.420E+06	5.496E+06	2.850E-05	2.814E-05	2.853E-05	9.784E-02	9.660E-02	9.796E-02	B+
11	1	190	8.31912E+01	E1	9.156E-03	4.722E+08	4.672E+08	4.686E+08	1.470E-03	1.455E-03	1.458E-03	4.026E-04	3.984E-04	3.994E-04	B+
11	1	196	8.29666E+01	E1	9.673E-02	7.737E+08	7.800E+08	7.596E+08	2.395E-03	2.415E-03	2.352E-03	6.542E-04	6.596E-04	6.423E-04	B+
11	1	201	8.27823E+01	E2	9.625E-05	4.294E+06	4.268E+06	4.254E+06	2.206E-05	2.192E-05	2.185E-05	7.454E-02	7.406E-02	7.384E-02	B+
11	1	204	8.27060E+01	E1	3.970E-03	4.888E+07	4.828E+07	4.794E+07	1.504E-04	1.485E-04	1.475E-04	4.095E-05	4.044E-05	4.015E-05	B+
11	1	212	8.21649E+01	E2	2.074E-05	2.510E+05	2.369E+05	2.742E+05	1.270E-06	1.199E-06	1.388E-06	4.196E-03	3.961E-03	4.584E-03	B+
11	1	228	8.15659E+01	E1	6.853E-03	3.607E+07	3.334E+07	3.595E+07	1.079E-04	9.978E-05	1.076E-04	2.898E-05	2.679E-05	2.889E-05	B
11	1	230	8.15224E+01	E1	5.447E-01	3.060E+10	2.970E+10	3.048E+10	9.147E-02	8.878E-02	9.112E-02	2.455E-02	2.383E-02	2.445E-02	A
11	1	234	8.14825E+01	E1	5.122E-01	1.278E+10	1.397E+10	1.269E+10	3.815E-02	4.173E-02	3.789E-02	1.023E-02	1.120E-02	1.016E-02	B
11	1	240	8.13664E+01	E1	1.652E-02	6.382E+08	6.468E+08	6.353E+08	1.900E-03	1.926E-03	1.892E-03	5.090E-04	5.160E-04	5.068E-04	B+

Table 3
(Continued)

Z	i	j	λ	Type	BF	A_l(AS$_5$)	A_l(AS$_4$)	A_v(AS$_5$)	gf_l(AS$_5$)	gf_l(AS$_4$)	gf_v(AS$_5$)	S_l(AS$_5$)	S_l(AS$_4$)	S_v(AS$_5$)	Acc.
11	1	249	8.12022E+01	E1	3.841E-02	1.666E+09	1.654E+09	1.656E+09	4.940E-03	4.906E-03	4.912E-03	1.321E-03	1.312E-03	1.313E-03	B+
11	1	251	8.11408E+01	E1	1.021E-01	3.674E+09	3.677E+09	3.666E+09	1.088E-02	1.089E-02	1.086E-02	2.906E-03	2.909E-03	2.900E-03	B+
11	1	256	8.10968E+01	E2	1.180E-05	2.972E+05	2.842E+05	3.245E+05	1.465E-06	1.401E-06	1.600E-06	4.655E-03	4.452E-03	5.082E-03	B+
11	1	271	8.09277E+01	E1	1.858E-01	4.503E+09	4.537E+09	4.503E+09	1.326E-02	1.336E-02	1.326E-02	3.534E-03	3.561E-03	3.534E-03	B+

Notes. A_l(AS$_5$), gf_l(AS$_5$), and S_l(AS$_5$) are, respectively, transition rates, weighted oscillator strengths, and line strengths in the length (l) form from the present MCDHF calculations based on AS_5. A_l(AS$_4$), gf_l(AS$_4$), and S_l(AS$_4$) are, respectively, transition rates, weighted oscillator strengths, and line strengths in the length (l) form from the present MCDHF calculations based on AS_4. A_v(AS$_5$), gf_v(AS$_5$), and S_v(AS$_5$) are, respectively, transition rates, weighted oscillator strengths, and line strengths in the velocity (v) form from the present MCDHF calculations. Type is the type of the multipole, and BF is the branching fraction from the upper level. The last column (Acc.) represents the estimated accuracies of the S values using the terminologies of the NIST database. Only transitions with BF $\geqslant 10^{-5}$ are presented. Part of the values for Na VI are shown here for guidance regarding their form and content.

(This table is available in its entirety in machine-readable form.)

Table 4

Excitation Energies E in cm^{-1} for 156 States of O III from the Present MCDHF Calculations (Hereafter MCDHF)

Z	Key	Level	E						ΔE				
			NIST	MCDHF	MCDHF1	MCHF	MCHF1	AUTOSTRUCTURE	MCDHF	MCDHF1	MCHF	MCHF1	AUTOSTRUCTURE
8	1	$2s^22p^2\ ^3P_0$	0	0	0	0	0	0	0	0	0	0	0
8	2	$2s^22p^2\ ^3P_1$	113.178	110.60	113.6	113.37	113	126	−2.578	0.422	0.192	−0.178	12.822
8	3	$2s^22p^2\ ^3P_2$	306.174	303.54	305.0	305.60	331	343	−2.634	−1.174	−0.574	24.826	36.826
8	4	$2s^22p^2\ ^1D_2$	20,273.27	20,351.7	20,400.4	20,369.35	20,309	22,931	78.43	127.13	96.08	35.73	2657.73
8	5	$2s^22p^2\ ^1S_0$	43,185.74	43,324.2	43,393.4	43,278.14	43183	56283	138.46	207.66	92.40	−2.74	13,097.26
8	6	$2s2p^3\ ^5S_2^\circ$	60,324.79	60,255.9	60,022.8	60,531.59	60250	43452	−68.89	−301.99	206.80	−74.79	−16,872.79
8	7	$2s2p^3\ ^3D_3^\circ$	120,025.2	120,185	120,098.9	120,464.4	120,120	117,794	159.8	73.7	439.2	94.8	−2231.2
8	8	$2s2p^3\ ^3D_2^\circ$	120,053.4	120,208	120,125.8	120,492.2	120,128	117,829	154.6	72.4	438.8	74.6	−2224.4
8	9	$2s2p^3\ ^3D_1^\circ$	120,058.2	120,214	120,131.4	120,497.7	120,128	117,840	155.8	73.2	439.5	69.8	−2218.2
8	10	$2s2p^3\ ^3P_2^\circ$	142,381.0	142,601	142,647.7	142,903.3	142,704	140,554	220	266.7	522.3	323.0	−1827
8	11	$2s2p^3\ ^3P_1^\circ$	142,381.8	142,603	142,649.6	142,905.3	142,704	140,896	221.2	267.8	523.5	322.2	−1485.8
8	12	$2s2p^3\ ^3P_0^\circ$	142,393.5	142,629	142,669.7	142,919.3	142,712	140,894	235.5	276.2	525.8	318.5	−1499.5
8	13	$2s2p^3\ ^1D_2^\circ$	187,054.0	187,422	187,366.5	187,666.3	187,298	198,702	368	312.5	612.3	244.0	11,648.0
8	14	$2s2p^3\ ^3S_1^\circ$	197,087.7	197,401	197,299.5	197,581.2	197,525	206,534	313.3	211.8	493.5	437.3	9446.3
8	15	$2s2p^3\ ^1P_1^\circ$	210,461.8	210,920	211,171.1	211,184.4	211,051	220,928	458.2	709.3	722.6	589.2	10,466.2
8	16	$2s^22p3s\ ^3P_0^\circ$	267,258.71	267,120		267,842.0	267,316	266,005	−138.71		583.29	57.29	−1253.71
8	17	$2s^22p3s\ ^3P_1^\circ$	267,377.11	267,233		267,960.1	267,437	266,122	−144.11		582.99	59.89	−1255.11
8	18	$2s^22p3s\ ^3P_2^\circ$	267,634.00	267,491		268,216.0	267,687	266,374	−143		582.00	53.00	−1260.00
8	19	$2s^22p3s\ ^1P_1^\circ$	273,081.33	272,971		273,720.2	273,374	272,208	−110.33		638.87	292.67	−873.33
8	20	$2p^4\ ^3P_2$	283,759.70	284,208		284,695.5	284,020		448.3		935.8	260.30	
8	21	$2p^4\ ^3P_1$	283,977.40	284,425		284,911.5	284,222		447.6		934.1	244.60	
8	22	$2p^4\ ^3P_0$	284,071.90	284,541		285,005.6	284,318		469.1		933.7	246.10	
8	23	$2s^22p3p\ ^1P_1$	290,958.25	290,832		291,672.6	290,916	290,602	−126.25		714.35	−42.25	−356.25
8	24	$2s^22p3p\ ^3D_1$	293,866.49	293,741		294,577.4	293,868	292,737	−125.49		710.91	1.51	−1129.49
8	25	$2s^22p3p\ ^3D_2$	294,002.86	293,879		294,712.8	294,005	292,871	−123.86		709.94	2.14	−1131.86
8	26	$2s^22p3p\ ^3D_3$	294,223.07	294,103		294,931.6	294,215	293,089	−120.07		708.53	−8.07	−1134.07
8	27	$2s^22p3p\ ^3S_1$	297,558.66	297,426		298,229.4	297,546	296,408	−132.66		670.74	−12.66	−1150.66
8	28	$2p^4\ ^1D_2$	298,294.0	298,908		299,391.6	298,554		614		1097.6	260.0	
8	29	$2s^22p3p\ ^3P_0$	300,229.93	300,128		300,907.2	300,425	301,628	−101.93		677.27	195.07	1398.07
8	30	$2s^22p3p\ ^3P_1$	300,311.96	300,206		300,988.7	300,506	301,707	−105.96		676.74	194.04	1395.04
8	31	$2s^22p3p\ ^3P_2$	300,442.55	300,337		301,118.1	300,643	301,845	−105.55		675.55	200.45	1402.45
8	32	$2s^22p3p\ ^1D_2$	306,586.08	306,543		307,322.0	306,902	307,282	−43.08		735.92	315.92	695.92
8	33	$2s^22p3p\ ^1S_0$	313,802.77	313,831		314,671.4	314,226	315,362	28.23		868.63	423.23	1559.23
8	34	$2s^22p3d\ ^3F_2^\circ$	324,464.88	324,423		325,112.6	324,461	322,962	−41.88		647.72	−3.88	−1502.88
8	35	$2s^22p3d\ ^3F_3^\circ$	324,660.80	324,634		325,312.8	324,695	323,111	−26.8		652	34.20	−1549.80
8	36	$2s^22p3d\ ^1D_2^\circ$	324,735.65	324,694		325,374.6	324,703	323,651	−41.65		638.95	−32.65	−1084.65
8	37	$2s^22p3d\ ^3F_4^\circ$	324,839.03	324,825		325,490.7	324,872	323,291	−14.03		651.67	32.97	−1548.03
8	38	$2s^22p3d\ ^3D_1^\circ$	327,229.25	327,167		327,828.1	327,001	326,276	−62.25		598.85	−228.25	−953.25
8	39	$2s^22p3d\ ^3D_2^\circ$	327,278.30	327,220		327,877.0	327,050	326,324	−58.3		598.7	−228.30	−954.30
8	40	$2s^22p3d\ ^3D_3^\circ$	327,352.17	327,300		327,950.4	327,122	326,400	−52.17		598.23	−230.17	−952.17
8	41	$2s^22p3d\ ^3P_2^\circ$	329,469.80	329,409		330,077.9	329,413	328,207	−60.8		608.1	−56.80	−1262.80
8	42	$2s^22p3d\ ^3P_1^\circ$	329,583.89	329,517		330,192.2	329,518	328,317	−66.89		608.31	−65.89	−1266.89
8	43	$2s^22p3d\ ^3P_0^\circ$	329,645.14	329,582		330,253.8	329,574	328,372	−63.14		608.66	−71.14	−1273.14
8	44	$2s^22p3d\ ^1F_3^\circ$	331,821.44	331,825		332,452.6	331,784	332,217	3.56		631.16	−37.44	395.56
8	45	$2s^22p3d\ ^1P_1^\circ$	332,778.94	332,748		333,420.7	332,825	333,332	−30.94		641.76	46.06	553.06
8	46	$2s2p^2(^3P)3s\ ^5P_1$	338,577.25	338,427			338,777		−150.25			199.75	

Table 4
(Continued)

Z	Key	Level	E						ΔE				
			NIST	MCDHF	MCDHF1	MCHF	MCHF1	AUTOSTRUCTURE	MCDHF	MCDHF1	MCHF	MCHF1	AUTOSTRUCTURE
8	47	$2s2p^2(^3P)3s\ ^5P_2$	338,701.98	338,551			338,906		−150.98			204.02	
8	48	$2s2p^2(^3P)3s\ ^5P_3$	338,863.03	338,716			339,100		−147.03			236.97	
8	49	$2p^4\ ^1S_0$	343,306.3	344,147		344,761.7	343,826		840.7		1455.4	519.7	
8	50	$2s2p^2(^3P)3s\ ^3P_0$	350,024.49	349,990			350,633		−34.49			608.51	
8	51	$2s2p^2(^3P)3s\ ^3P_1$	350,124.45	350,088			350,730		−36.45			605.55	
8	52	$2s2p^2(^3P)3s\ ^3P_2$	350,298.38	350,261			350,932		−37.38			633.62	
8	53	$2s^22p4s\ ^3P_0°$	356,736.30	356,640			356,199	354,061	−96.3			−537.30	−2675.30
8	54	$2s^22p4s\ ^3P_1°$	356,844.98	356,744			356,303	354,168	−100.98			−541.98	−2676.98
8	55	$2s^22p4s\ ^3P_2°$	357,117.01	357,016			356,570	354,435	−101.01			−547.01	−2682.01
8	56	$2s^22p4s\ ^1P_1°$	358,668.90	358,634			358,199	355,950	−34.9			−469.90	−2718.90
8	57	$2s2p^2(^3P)3p\ ^3S_1°$	363,263.38	363,163			363,079		−100.38			−184.38	
8	58	$2s2p^2(^3P)3p\ ^5D_0°$	365,527.08	365,416			365,498		−111.08			−29.08	
8	59	$2s2p^2(^3P)3p\ ^5D_1°$	365,561.95	365,449			365,539		−112.95			−22.95	
8	60	$2s2p^2(^3P)3p\ ^5D_2°$	365,630.40	365,518			365,611		−112.4			−19.40	
8	61	$2s^22p4p\ ^1P_1$	365,726.76	365,598			365,168	364,084	−128.76			−558.76	−1642.76
8	62	$2s2p^2(^3P)3p\ ^5D_3°$	365,730.68	365,622			365,716		−108.68			−14.68	
8	63	$2s2p^2(^3P)3p\ ^5D_4°$	365,857.89	365,754			365,869		−103.89			11.11	
8	64	$2s^22p4p\ ^3D_1$	366,488.45	366,377			365,958	364,606	−111.45			−530.45	−1882.45
8	65	$2s^22p4p\ ^3D_2$	366,595.76	366,485			366,063	364,704	−110.76			−532.76	−1891.76
8	66	$2s^22p4p\ ^3D_3$	366,802.62	366,694			366,264	364,911	−108.62			−538.62	−1891.62
8	67	$2s^22p4p\ ^3S_1$	367,953.90	367,869			367,434	365,794	−84.9			−519.90	−2159.90
8	68	$2s2p^2(^3P)3p\ ^5P_1°$	368,538.65	368,415			368,611		−123.65			72.35	
8	69	$2s2p^2(^3P)3p\ ^5P_2°$	368,595.93	368,472			368,684		−123.93			88.07	
8	70	$2s2p^2(^3P)3p\ ^5P_3°$	368,697.00	368,576			368,797		−121			100.00	
8	71	$2s^22p4p\ ^3P_0$	370,329.18	370,426			370,055	367,132	96.82			−274.18	−3197.18
8	72	$2s^22p4p\ ^3P_1$	370,418.32	370,510			370,144	367,223	91.68			−274.32	−3195.32
8	73	$2s^22p4p\ ^3P_2$	370,526.49	370,619			370,249	367,339	92.51			−277.49	−3187.49
8	74	$2s^22p4p\ ^1D_2$	370,902.22	371,012			370,539	369,506	109.78			−363.22	−1396.22
8	75	$2s^22p4p\ ^1S_0$		374,237			373,548	373,658					
8	76	$2s2p^2(^3P)3p\ ^3D_1°$	374,571.64	374,531			374,846		−40.64			274.36	
8	77	$2s2p^2(^3P)3p\ ^3D_2°$	374,663.52	374,622			374,943		−41.52			279.48	
8	78	$2s2p^2(^3P)3p\ ^3D_3°$	374,795.14	374,757			375,088		−38.14			292.86	
8	79	$2s2p^2(^3P)3p\ ^5S_2°$	376,079.92	376,016			376,435		−63.92			355.08	
8	80	$2s^22p4d\ ^3F_2°$	377,385.58	377,259			376,895		−126.58			−490.58	
8	81	$2s^22p4d\ ^3F_3°$	377,562.31	377,440			377,080		−122.31			−482.31	
8	82	$2s^22p4d\ ^1D_2°$	377,686.83	377,562			377,169		−124.83			−517.83	
8	83	$2s^22p4d\ ^3F_4°$	377,748.57	377,630			377,266		−118.57			−482.57	
8	84	$2s^22p4d\ ^3P_2°$	378,405.68	378,320			378,185		−85.68			−220.68	
8	85	$2s^22p4d\ ^3P_1°$	378,417.84	378,337			378,234		−80.84			−183.84	
8	86	$2s2p^2(^3P)3p\ ^3P_0°$	378,435.16	378,362			380,815		−73.16			2379.84	
8	87	$2s^22p4d\ ^3D_1°$	379,227.15	379,128			378,887		−99.15			−340.15	
8	88	$2s^22p4d\ ^3D_2°$	379,293.03	379,195			378,960		−98.03			−333.03	
8	89	$2s^22p4d\ ^3D_3°$	379,356.75	379,261			379,024		−95.75			−332.75	
8	90	$2s^22p4f\ ^3F_2$	380,621.90	380,530			379,952		−91.9			−669.90	
8	91	$2s^22p4f\ ^1F_3$	380,612.20	380,532			379,936		−80.2			−676.20	
8	92	$2s^22p4f\ ^3F_3$	380,671.30	380,578			380,000		−93.3			−671.30	

Table 4
(Continued)

Z	Key	Level	E						ΔE				
			NIST	MCDHF	MCDHF1	MCHF	MCHF1	AUTOSTRUCTURE	MCDHF	MCDHF1	MCHF	MCHF1	AUTOSTRUCTURE
8	93	$2s^22p4f\ ^3F_4$	380,685.90	380,610			380,016		−75.9			−669.90	
8	94	$2s2p^2(^3P)3p\ ^3P_2^\circ$	380,706.51	380,704			380,936		−2.51			229.49	
8	95	$2s2p^2(^3P)3p\ ^3P_1^\circ$	380,717.92	380,709			380,911		−8.92			193.08	
8	96	$2s^22p4d\ ^3P_0^\circ$	380,737.00	380,732			378,266		−5			−2471.00	
8	97	$2s^22p4d\ ^1F_3^\circ$	380,782.17	380,746			380,992		−36.17			209.83	
8	98	$2s^22p4d\ ^1P_1^\circ$	381,089.27	381,057			380,274		−32.27			−815.27	
8	99	$2s^22p4f\ ^3G_3$	381,176.90	381,092			381,008		−84.9			−168.90	
8	100	$2s^22p4f\ ^3G_4$	381,211.30	381,142			381,041		−69.3			−170.30	
8	101	$2s^22p4f\ ^3G_5$	381,404.50	381,339			380,637		−65.5			−767.50	
8	102	$2s^22p4f\ ^3D_3$	381,456.80	381,365			380,516		−91.8			−940.80	
8	103	$2s^22p4f\ ^3D_2$	381,477.80	381,375			380,549		−102.8			−928.80	
8	104	$2s^22p4f\ ^1G_4$	381,472.50	381,393			380,742		−79.5			−730.50	
8	105	$2s^22p4f\ ^3D_1$	381,623.80	381,522			380,750		−101.8			−873.80	
8	106	$2s^22p4f\ ^1D_2$	381,645.00	381,557			380,774		−88			−871.00	
8	107	$2s^22p5s\ ^3P_0^\circ$	391,830.76	391,736			391,179	388,441	−94.76			−651.76	−3389.76
8	108	$2s^22p5s\ ^3P_1^\circ$	391,917.80	391,821			391,268	388,530	−96.8			−649.80	−3387.80
8	109	$2s^22p5s\ ^3P_2^\circ$	392,209.53	392,110			391,550	388,816	−99.53			−659.53	−3393.53
8	110	$2s^22p5s\ ^1P_1^\circ$	392,781.47	392,753			392,155	389,427	−28.47			−626.47	−3354.47
8	111	$2s2p^2(^1D)3s\ ^3D_1$	394,079.4	394,069			398,486		−10.4			4406.6	
8	112	$2s2p^2(^1D)3s\ ^3D_2$	394,127.3	394,123			398,559		−4.3			4431.7	
8	113	$2s2p^2(^1D)3s\ ^3D_3$	394,197.9	394,209			398,131		11.1			3933.1	
8	114	$2s2p^2(^3P)3d\ ^5F_1$	394,528.20	394,462			394,720		−66.2			191.80	
8	115	$2s2p^2(^3P)3d\ ^5F_2$	394,567.05	394,503			394,768		−64.05			200.95	
8	116	$2s2p^2(^3P)3d\ ^5F_3$	394,624.68	394,567			394,833		−57.68			208.32	
8	117	$2s2p^2(^3P)3d\ ^5F_4$	394,700.27	394,654			394,921		−46.27			220.73	
8	118	$2s2p^2(^3P)3d\ ^5F_5$	394,793.28	394,757			395,034		−36.28			240.72	
8	119	$2s^22p5p\ ^1P_1$		395,976									
8	120	$2s^22p5p\ ^3S_1$		397,054									
8	121	$2s^22p5p\ ^1D_2$		397,904									
8	122	$2s^22p5p\ ^3P_0$		397,909									
8	123	$2s^22p5p\ ^3P_1$		397,990									
8	124	$2s2p^2(^3P)3d\ ^5D_2$	398,139.92	398,038			398,260		−101.92			120.08	
8	125	$2s2p^2(^3P)3d\ ^5D_1$	398,144.29	398,039			398,285		−105.29			140.71	
8	126	$2s2p^2(^3P)3d\ ^5D_0$	398,145.63	398,045			398,212		−100.63			66.37	
8	127	$2s2p^2(^3P)3d\ ^5D_3$	398,150.40	398,052			398,333		−98.4			182.60	
8	128	$2s2p^2(^3P)3d\ ^5D_4$	398,231.48	398,140			398,414		−91.48			182.52	
8	129	$2s^22p5p\ ^3P_2$		398,144									
8	130	$2s^22p5p\ ^3D_1$		398,278									
8	131	$2s^22p5p\ ^3D_2$		398,378									
8	132	$2s2p^2(^3P)3d\ ^5P_3$	398,487.08	398,382			398,438		−105.08			−49.08	
8	133	$2s2p^2(^3P)3d\ ^5P_2$	398,557.17	398,450			398,527		−107.17			−30.17	
8	134	$2s^22p5p\ ^3D_3$		398,457									
8	135	$2s2p^2(^3P)3d\ ^5P_1$	398,595.65	398,486			398,551		−109.65			−44.65	
8	136	$2s2p^2(^3P)3d\ ^3P_2$	400,351.56	400,289			400,462		−62.56			110.44	
8	137	$2s2p^2(^3P)3d\ ^3P_1$	400,460.99	400,402			400,583		−58.99			122.01	
8	138	$2s2p^2(^3P)3d\ ^3P_0$	400,514.89	400,466			400,640		−48.89			125.11	

Table 4
(Continued)

Z	Key	Level	E						ΔE				
			NIST	MCDHF	MCDHF1	MCHF	MCHF1	AUTOSTRUCTURE	MCDHF	MCDHF1	MCHF	MCHF1	AUTOSTRUCTURE
8	139	$2s^22p5p\ ^1S_0$		401,102									
8	140	$2s2p^2(^3P)3d\ ^3F_2$	401,375.09	401,349			401,479		−26.09			103.91	
8	141	$2s^22p5d\ ^3F_2^{\circ}$	401,519.8	401,386					−133.8				
8	142	$2s2p^2(^3P)3d\ ^3F_3$	401,476.29	401,448			401,592		−28.29				
8	143	$2s^22p5d\ ^3F_3^{\circ}$	401,725.6	401,557					−168.6				
8	144	$2s2p^2(^3P)3d\ ^3F_4$	401,605.52	401,578			401,737		−27.52				
8	145	$2s^22p5d\ ^1D_2^{\circ}$	401,791.7	401,659					−132.7				
8	146	$2s^22p5d\ ^3F_4^{\circ}$	401,893.2	401,763					−130.2				
8	147	$2s^22p5d\ ^3D_1^{\circ}$		402,229									
8	148	$2s^22p5d\ ^3D_2^{\circ}$	402,411.5	402,283					−128.5				
8	149	$2s^22p5d\ ^3D_3^{\circ}$	402,533.3	402,401					−132.3				
8	150	$2s^22p5d\ ^3P_2^{\circ}$		402,642									
8	151	$2s^22p5d\ ^3P_1^{\circ}$		402,715									
8	152	$2s^22p5d\ ^3P_0^{\circ}$		402,757									
8	153	$2s^22p5f\ ^1F_3$		403,077									
8	154	$2s^22p5f\ ^3F_2$		403,086									
8	155	$2s^22p5f\ ^3F_3$		403,105									
8	156	$2s^22p5f\ ^3F_4$		403,136									

Note. Besides the present MCDHF excitation energies, the calculations by Jönsson & Bieroń (2010), Jönsson et al. (2011) (hereafter referred to as MCDHF1), by Tachiev & Froese Fischer (2001), Froese Fischer & Tachiev (2004) (MCHF), by Tayal & Zatsarinny (2017) (MCHF1), and by Al-Modlej et al. (2018) (AUTOSTRUCTURE) are also provided, as well as the compiled values E_{NIST} from the NIST database (Kramida et al. 2020), The differences ($\Delta E_x = E_x - E_{\mathrm{NIST}}$) in cm^{-1} of different calculations from the compiled values E_{NIST} are listed.

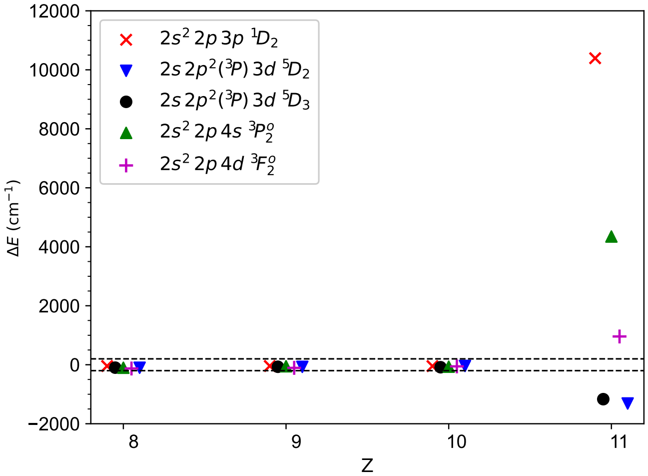

Figure 1. The energy differences $\Delta E = E_{\rm MCDHF} - E_{\rm NIST}$ (in cm^{-1}) for the $2s^2\,2p\,3p\ \ ^1D_2$, $2s\,2p^2(^3P)3d\ \ ^5D_2$, $2s\,2p^2(^3P)3d\ \ ^5D_3$, $2s^2\,2p\,4s\ \ ^3P_2{}^\circ$, and $2s^2\,2p\,4d\ \ ^3F_2{}^\circ$ states as functions of the nuclear charge Z. The data for all states are available in Table 2. Experiment and theory agree very well for the states in O III, F IV, and Ne V, but for the states in Na VI there are large discrepancies.

3.2. Line Identifications for Na VI

To revise the identifications in Na VI, a list of the strongest Na VI lines from the transition arrays $n = 5$, 4, $3 \to n = 2$ in the wavelength range from 80 to 150 Å is provided in Table 5. Using the present atomic data (wavelengths $\lambda_{\rm MCDHF}$ and transition rates $A_{\rm MCDHF}$) and electron-impact excitation data provided by Mao et al. (2020), relative intensities (photons) $Int = N_j A_{ji}/N_{\rm e}$ are calculated at a fixed temperature T_e [K] $= 4 \times 10^5$, and at low and high electron densities N_e [cm^{-3}] $= 10^9$ and 10^{13}, typical of the quiet solar corona and of laboratory spectra. The experimental wavelengths, which were compiled in the NIST database by Sansonetti (2008), were observed by Söderqvist (1946). The uncertainties displayed in the NIST database for all lines from Söderqvist (1946) are about 0.01 Å.

3.2.1. The n = 5 → n = 2 Lines

For the $5d \to 2p$ transition, lines in the wavelength range from 81 to 86 Å are shown in Table 5. The experimental wavelengths of 81.543 Å (#3–#238) and 83.639 Å (#4–#246) identified by Söderqvist (1946) and compiled in the NIST database by Sansonetti (2008) agree well with the present values $\lambda_{\rm MCDHF}$ of 81.527 and 83.634 Å, respectively.

One unassigned line observed by Söderqvist (1946) at 81.498 Å is in good agreement with our MCDHF value $\lambda_{\rm MCDHF} = 81.499$ Å for the transition $\#3/2s^2\,2p^2\ {}^3P_2$–$\#239/2s^2\,2p\,5d\ \ ^3P_2{}^\circ$. Meanwhile, the predicted relative intensities of this line 81.498 Å are strong at both low and high plasma densities. Hence, we suggest assigning the line at 81.498 Å to the transition #3–#239. Using this new identification at 81.498 Å and the experimental excitation energy 1855.98 cm^{-1} for the lower level $\#3/2s^2\,2p^2\ \ ^3P_2$, the experimental value for the upper level $\#239/2s^2\,2p\,5d\ \ ^3P_2{}^\circ$ should then be 1,228,880 cm^{-1}. This new excitation energy shows excellent agreement (within 40 cm^{-1}) with our MCDHF computed excitation energy of 1,228,857 cm^{-1}.

The above comparison for the three strongest $5d \to 2p$ lines (81.498, 81.543, and 83.639 Å) implies that the present MCDHF calculations reach spectroscopic accuracy, and can be used to identify yet unidentified observed lines.

Söderqvist (1946) observed a line at 111.725 Å, and assigned this line to the transition $\#4/2s^2\,2p^2\ \ ^1D_2$–$\#44/2s^2\,2p\,3d\ \ ^3D_3{}^\circ$. As shown in Table 5, the predicted intensities of this transition $\#4/2s^2\,2p^2\ \ ^1D_2$–$\#44/2s^2\,2p\,3d\ \ ^3D_3{}^\circ$ are not very high at either low or high plasma densities. By contrast, the relative intensity of one $n = 5 \to n = 2$ transition (#210 → #14) is one order of magnitude larger than the intensity of the transition #44 → #4 at both low and high plasma densities. This line at 111.725 Å is also in good agreement with our MCDHF wavelength $\lambda_{\rm MCDHF} = 111.732$ Å for the latter transition. Hence, we tentatively assign the line at 111.725 Å to the transition $\#14/2s\,2p^3\ \ ^3S_1{}^\circ$–$\#210/2s^2\,2p\,5p\ \ ^1P_1$.

3.2.2. The n = 4 → n = 2 Lines

Among the $n = 4 \to n = 2$ lines, the ones from the $2s^22p4d$ configuration are the most prominent in the X-ray wavelength range from 88 to 94 Å. For the strongest lines of the $2s^22p4d \to 2s^22p^2$ transition array shown in Table 5, the wavelengths of 88.143 Å (#3–#150), 88.223 Å (#1–#138), 88.246 Å (#2–#139), 88.270 Å (#3–#144), 88.340 Å (#3–#139), 90.468 Å (#4–#155), and 91.268 Å (#4–#136), identified by Söderqvist (1946), agree well with our MCDHF values $\lambda_{\rm MCDHF}$ of 88.134 Å, 88.223 Å, 88.250 Å, 88.276 Å, 88.340 Å, 90.474 Å, and 91.277 Å, respectively. The corresponding excitation energies for the $2s^22p4d$ states (#136, #138, #139, #144, #150, and #155) listed in the NIST database are confirmed, as the energy differences from our MCDHF results included in Table 2 are within 120 cm^{-1}.

However, the identification of one line 88.583 Å by Söderqvist (1946) is questionable. Although the wavelength 88.583 Å assigned to the $\#3/2s^2\,2p^2\ {}^3P_2$–$\#136/2s^2\,2p\,4d\ {}^1D_2{}^\circ$ transition is comparatively close to the MCDHF value ($\lambda_{\rm MCDHF} =$ 88.550 Å), the intensity of this transition #3–#136 is two orders of magnitude smaller than the intensity of the $\#3/2s^2\,2p^2\ \ ^3P_2$–$\#135/2s^2\,2p\,4d\ \ ^3F_3{}^\circ$ transition associated with the MCDHF wavelength ($\lambda_{\rm MCDHF} =$ 88.596 Å) at both low and high plasma densities. The dubious identification exists for the line 88.038 Å as well. Although the wavelength 88.038 Å assigned to the $\#2/2s^2\,2p^2\ \ ^3P_1$–$\#150/2s^2\,2p\,4d\ \ ^3P_2{}^\circ$ transition is close to the MCDHF value ($\lambda_{\rm MCDHF} = 88.053$ Å), the relative intensities for this transition (#2–#150) at both low and high plasma densities are much smaller than the relative intensities of the $\#2/2s^2\,2p^2\ \ ^3P_1$–$\#151/2s^2\,2p\,4d\ \ ^3P_1{}^\circ$ transition, associated with the MCDHF wavelength ($\lambda_{\rm MCDHF} = 88.038$ Å). Therefore, we suggest to assign the lines 88.583 Å and 88.038 Å to the transitions $\#3/2s^2\,2p^2\ \ ^3P_2$–$\#135/2s^2\,2p\,4d\ \ ^3F_3{}^\circ$ and $\#2/2s^2\,2p^2\ \ ^3P_1$–$\#151/2s^2\,2p\,4d\ \ ^3P_1{}^\circ$, respectively.

One unassigned line observed by Söderqvist (1946) at 81.584 Å is in good agreement with our MCDHF value $\lambda_{\rm MCDHF} = 81.579$ Å for the transition $\#3/2s^2\,2p^2\ {}^3P_2$–$\#235/2s\,2p^2(^3P)4p\ \ ^3D_3{}^\circ$. The predicted relative intensities of this line 81.584 Å are strong at both low and high plasma densities. Hence, we suggest assigning the line at 81.584 Å to the transition #3–#235. Using this new identification at 81.584 Å and the experimental excitation energy 1855.98 cm^{-1} for the lower level $\#3/2s^2\,2p^2\ \ ^3P_2$, the experimental value for the upper level $\#235/2s\,2p^2(^3P)4p\ \ ^3D_3{}^\circ$ should then be 1,227,586 cm^{-1}. This new excitation energy shows good agreement (within 8 0 cm^{-1}) with our MCDHF computed excitation energy of 1,227,660 cm^{-1}.

Table 5
A List of the Strongest Na VI Lines from the Transition Arrays $n = 5, 4, 3 \rightarrow n = 3$ in the Wavelength Range from 80 to 150 Å

i–j	Transition	Int (10^9)	Int (10^{13})	$\lambda_{\rm NIST}$	$\lambda_{\rm MCDHF}$	$\lambda_{\rm rev}$	$A_{\rm MCDHF}$	Note
2–240	$2s^22p^2\ ^3P_1$–$2s^22p5d\ ^3P_1^\circ$	7.05E-03	7.15E-03		81.412		1.857E+10	
1–234	$2s^22p^2\ ^3P_0$–$2s^22p\ 5d\ ^3D_1^\circ$	9.96E-03	1.03E-02		81.483		1.278E+10	
3–240	$2s^22p^2\ ^3P_2$–$2s^22p\ 5d\ ^3P_1^\circ$	4.97E-03	5.04E-03		81.489		1.310E+10	
2–236	$2s^22p^2\ ^3P_1$–$2s^22p\ 5d\ ^3D_2^\circ$	1.44E-02	1.47E-02		81.497		1.487E+10	
3–239	$2s^22p^2\ ^3P_2$–$2s^22p\ 5d\ ^3P_2^\circ$	2.07E-02	2.09E-02		81.499	81.498	3.100E+10	N
3–238	$2s^22p^2\ ^3P_2$–$2s^22p\ 5d\ ^3D_3^\circ$	3.45E-02	3.44E-02	81.543	81.527 (−0.016)		2.555E+10	
2–233	$2s^22p^2\ ^3P_1$–$2s\ 2p^2(^3P)4p\ ^3D_2^\circ$	4.75E-03	5.30E-03		81.538		2.252E+10	
3–235	$2s^22p^2\ ^3P_2$–$2s\ 2p^2(^3P)4p\ ^3D_3^\circ$	8.03E-03	9.09E-03		81.579	81.584	3.001E+10	N
2–227	$2s^22p^2\ ^3P_1$–$2s^22p\ 5d\ ^1D_2^\circ$	8.71E-03	9.56E-03		81.613		1.460E+10	
4–246	$2s^22p^2\ ^1D_2$–$2s^22p\ 5d\ ^1F_3^\circ$	4.19E-02	5.52E-02	83.639	83.634 (−0.005)		6.022E+10	
5–249	$2s^22p^2\ ^1S_0$–$2s^22p\ 5d\ ^1P_1^\circ$	6.80E-03	1.18E-02		86.439		3.395E+10	
2–151	$2s^22p^2\ ^3P_1$–$2s^22p\ 4d\ ^3P_1^\circ$	1.51E-02	1.55E-02		88.038	88.038	2.285E+10	N
2–150	$2s^22p^2\ ^3P_1$–$2s^22p\ 4d\ ^3P_2^\circ$	2.23E-03	2.29E-03	88.038 ?	88.043 (0.005)		1.512E+09	
2–149	$2s^22p^2\ ^3P_1$–$2s^22p\ 4d\ ^3P_0^\circ$	9.84E-03	1.00E-02		88.053		3.170E+10	
3–151	$2s^22p^2\ ^3P_2$–$2s^22p\ 4d\ ^3P_1^\circ$	1.57E-02	1.61E-02		88.128		2.377E+10	
3–150	$2s^22p^2\ ^3P_2$–$2s^22p\ 4d\ ^3P_2^\circ$	5.74E-02	5.92E-02	88.143	88.134 (−0.009)		3.905E+10	
1–138	$2s^22p^2\ ^3P_0$–$2s^22p\ 4d\ ^3D_1^\circ$	3.12E-02	3.27E-02	88.223	88.223 (0.000)		6.285E+10	
3–147	$2s^22p^2\ ^3P_2$–$2s\ 2p^2(^1S)3p\ ^3P_2^\circ$	1.31E-02	1.49E-02		88.237		2.728E+10	
2–139	$2s^22p^2\ ^3P_1$–$2s^22p\ 4d\ ^3D_2^\circ$	7.91E-02	7.84E-02	88.246	88.250 (0.004)		7.211E+10	
3–144	$2s^22p^2\ ^3P_2$–$2s^22p\ 4d\ ^3D_3^\circ$	1.34E-01	1.33E-01	88.270	88.276 (0.006)		9.941E+10	
2–138	$2s^22p^2\ ^3P_1$–$2s^22p\ 4d\ ^3D_1^\circ$	1.15E-02	1.20E-02		88.277		2.316E+10	
3–139	$2s^22p^2\ ^3P_2$–$2s^22p\ 4d\ ^3D_2^\circ$	1.81E-03	1.79E-03	88.340	88.340 (0.000)		1.649E+09	
3–136	$2s^22p^2\ ^3P_2$–$2s^22p\ 4d\ ^1D_2^\circ$	7.20E-05	8.47E-05	88.583 ?	88.550 (−0.033)		5.773E+07	
3–135	$2s^22p^2\ ^3P_2$–$2s^22p\ 4d\ ^3F_3^\circ$	8.19E-03	9.30E-03		88.596	88.583	3.017E+09	N
4–155	$2s^22p^2\ ^1D_2$–$2s^22p\ 4d\ ^1F_3^\circ$	1.05E-01	1.38E-01	90.468	90.474 (0.006)		1.058E+11	
6–194	$2s\ 2p^3\ ^5S_2^\circ$–$2s\ 2p^2(^3P)4s\ ^5P_3$	3.09E-03	5.62E-03	90.746 ?	90.830 (0.084)		1.083E+10	
4–136	$2s^22p^2\ ^1D_2$–$2s^22p\ 4d\ ^1D_2^\circ$	2.67E-02	3.13E-02	91.268	91.277 (0.009)		2.201E+10	
2–114	$2s^22p^2\ ^3P_1$–$2s^22p\ 4s\ ^3P_2^\circ$	7.34E-03	8.37E-03	91.737 ?	91.373 (−0.364)		3.135E+09	
3–114	$2s^22p^2\ ^3P_2$–$2s^22p\ 4s\ ^3P_2^\circ$	2.26E-02	2.58E-02	91.836 ?	91.470 (−0.366)		9.674E+09	
1–101	$2s^22p^2\ ^3P_0$–$2s\ 2p^2(^1D)3p\ ^3D_1^\circ$	3.12E-03	3.97E-03	96.124 ?	92.695 (−3.429)		1.466E+09	
2–101	$2s^22p^2\ ^3P_1$–$2s\ 2p^2(^1D)3p\ ^3D_1^\circ$	3.68E-03	4.69E-03	96.196 ?	92.755 (−3.441)		1.733E+09	
3–103	$2s^22p^2\ ^3P_2$–$2s\ 2p^2(^1D)3p\ ^3D_3^\circ$	1.05E-02	1.30E-02	96.307 ?	92.846 (−3.461)		3.059E+09	
5–161	$2s^22p^2\ ^1S_0$–$2s^22p\ 4d\ ^1P_1^\circ$	1.39E-02	2.40E-02		93.632		1.295E+10	
5–148	$2s^22p^2\ ^1S_0$–$2s\ 2p^2(^1S)3p\ ^1P_1^\circ$	1.16E-02	1.87E-02		94.205		9.961E+10	
4–107	$2s^22p^2\ ^1D_2$–$2s\ 2p^2(^1D)3p\ ^1P_1^\circ$	1.80E-02	2.38E-02		95.545		8.486E+10	
4–100	$2s^22p^2\ ^1D_2$–$2s\ 2p^2(^1D)3p\ ^1F_3^\circ$	4.37E-02	5.89E-02	96.475 ?	95.928 (−0.547)	95.933	6.885E+10	N
4–98	$2s^22p^2\ ^1D_2$–$2s\ 2p^2(^1D)3p\ ^1D_2^\circ$	2.91E-02	3.86E-02	95.933 ?	96.473 (0.540)	96.475	6.883E+10	N
1–67	$2s^22p^2\ ^3P_0$–$2s\ 2p^2(^3P)3p\ ^3P_1^\circ$	7.95E-03	9.06E-03	99.500	99.473 (−0.027)		1.302E+10	
2–68	$2s^22p^2\ ^3P_1$–$2s\ 2p^2(^3P)3p\ ^3P_2^\circ$	9.76E-03	1.11E-02	99.500	99.503 (0.003)		9.619E+09	
7–205	$2s\ 2p^3\ ^3D_3^\circ$–$2s\ 2p^2(^3P)4s\ ^3P_2$	4.13E-03	4.20E-03	99.004 ?	99.510 (0.506)		3.114E+09	
2–66	$2s^22p^2\ ^3P_1$–$2s\ 2p^2(^3P)3p\ ^3P_0^\circ$	8.61E-03	9.64E-03		99.562		4.372E+10	
3–68	$2s^22p^2\ ^3P_2$–$2s\ 2p^2(^3P)3p\ ^3P_2^\circ$	3.49E-02	3.98E-02	99.617	99.618 (0.001)		3.447E+10	
3–67	$2s^22p^2\ ^3P_2$–$2s\ 2p^2(^3P)3p\ ^3P_1^\circ$	1.20E-02	1.37E-02	99.680	99.657 (−0.023)		1.966E+10	
7–191	$2s\ 2p^3\ ^3D_3^\circ$–$2s\ 2p^2(^3P)3d\ ^3F_4$	1.66E-02	1.65E-02		100.201		3.931E+10	
8–189	$2s\ 2p^3\ ^3D_2^\circ$–$2s\ 2p^2(^3P)3d\ ^3F_3$	1.18E-02	1.16E-02		100.270		3.618E+10	
9–188	$2s\ 2p^3\ ^3D_1^\circ$–$2s\ 2p^2(^3P)3d\ ^3F_2$	7.04E-03	7.07E-03		100.281		2.942E+10	
1–62	$2s^22p^2\ ^3P_0$–$2s\ 2p^2(^3P)3p\ ^3D_1^\circ$	1.89E-02	2.20E-02		100.465		2.759E+10	
2–63	$2s^22p^2\ ^3P_1$–$2s\ 2p^2(^3P)3p\ ^3D_2^\circ$	4.29E-02	4.89E-02	100.469	100.481(0.012)		3.724E+10	
3–64	$2s^22p^2\ ^3P_2$–$2s\ 2p^2(^3P)3p\ ^3D_3^\circ$	7.75E-02	8.90E-02	100.519	100.518(−0.001)		4.755E+10	
2–62	$2s^22p^2\ ^3P_1$–$2s\ 2p^2(^3P)3p\ ^3D_1^\circ$	1.28E-02	1.49E-02		100.535		1.872E+10	
3–63	$2s^22p^2\ ^3P_2$–$2s\ 2p^2(^3P)3p\ ^3D_2^\circ$	1.17E-02	1.33E-02	100.590	100.598(0.008)		1.016E+10	
1–53	$2s^22p^2\ ^3P_0$–$2s\ 2p^2(^3P)3p\ ^3S_1^\circ$	5.82E-03	7.21E-03	103.002	103.024(0.022)		6.896E+09	
2–53	$2s^22p^2\ ^3P_1$–$2s\ 2p^2(^3P)3p\ ^3S_1^\circ$	1.68E-02	2.08E-02	103.078	103.097(0.019)		1.989E+10	
3–53	$2s^22p^2\ ^3P_2$–$2s\ 2p^2(^3P)3p\ ^3S_1^\circ$	2.62E-02	3.24E-02	103.210	103.221(0.011)		3.105E+10	
10–205	$2s\ 2p^3\ ^3P_2^\circ$–$2s\ 2p^2(^3P)4s\ ^3P_2$	1.05E-02	1.06E-02		103.345		8.190E+09	
10–203	$2s\ 2p^3\ ^3P_2^\circ$–$2s\ 2p^2(^3P)3d\ ^3D_3$	9.16E-03	9.07E-03		103.439		2.116E+10	
11–201	$2s\ 2p^3\ ^3P_1^\circ$–$2s\ 2p^2(^3P)3d\ ^3D_2$	5.80E-03	5.83E-03		103.470		2.039E+10	
6–85	$2s\ 2p^3\ ^5S_2^\circ$–$2s\ 2p^2(^3P)3d\ ^5P_1$	9.72E-03	6.73E-02	106.040	106.047(0.007)		2.767E+11	
6–84	$2s\ 2p^3\ ^5S_2^\circ$–$2s\ 2p^2(^3P)3d\ ^5P_2$	1.60E-02	1.11E-01	106.077	106.078(0.001)		2.738E+11	
6–83	$2s\ 2p^3\ ^5S_2^\circ$–$2s\ 2p^2(^3P)3d\ ^5P_3$	2.20E-02	1.55E-01	106.125	106.127(0.002)		2.734E+11	
7–164	$2s\ 2p^3\ ^3D_3^\circ$–$2s\ 2p^2(^1D)3d\ ^3P_2$	2.45E-03	3.00E-03	107.934?	106.478(−1.456)		4.820E+10	
8–160	$2s\ 2p^3\ ^3D_2^\circ$–$2s^22p\ 4f\ ^1D_2$	1.98E-04	2.70E-04		106.599	106.580	5.026E+08	N
6–81	$2s\ 2p^3\ ^5S_2^\circ$–$2s\ 2p^2(^3P)3d\ ^5D_3$	2.04E-02	2.86E-02	106.580?	106.701(0.121)		4.187E+09	
1–46	$2s^22p^2\ ^3P_0$–$2s^22p\ 3d\ ^3P_1^\circ$	5.21E-02	5.39E-02	107.014	107.022(0.008)		2.743E+10	

Table 5
(Continued)

i–j	Transition	Int (10^9)	Int (10^{13})	$\lambda_{\rm NIST}$	$\lambda_{\rm MCDHF}$	$\lambda_{\rm rev}$	$A_{\rm MCDHF}$	Note
2–47	$2s^22p^2\ ^3P_1$–$2s^22p\ 3d\ ^3P_0^\circ$	9.10E-02	9.28E-02	107.061	107.068(0.007)		1.434E+11	
2–46	$2s^22p^2\ ^3P_1$–$2s^22p\ 3d\ ^3P_1^\circ$	1.02E-01	1.06E-01	107.093	107.102(0.009)		5.376E+10	
2–45	$2s^22p^2\ ^3P_1$–$2s^22p\ 3d\ ^3P_2^\circ$	2.90E-02	2.98E-02	107.158	107.162(0.004)		9.121E+09	
3–46	$2s^22p^2\ ^3P_2$–$2s^22p\ 3d\ ^3P_1^\circ$	1.21E-01	1.26E-01	107.227	107.235(0.008)		6.405E+10	
3–45	$2s^22p^2\ ^3P_2$–$2s^22p\ 3d\ ^3P_2^\circ$	4.36E-01	4.49E-01	107.288	107.296(0.008)		1.376E+11	
7–140	$2s\ 2p^3\ ^3D_3^\circ$–$2s\ 2p^2(^1D)3d\ ^3D_3$	6.72E-03	8.49E-03		107.530	107.535	1.271E+11	N
1–42	$2s^22p^2\ ^3P_0$–$2s^22p\ 3d\ ^3D_1^\circ$	2.66E-01	2.71E-01	107.553	107.563(0.010)		1.607E+11	
2–43	$2s^22p^2\ ^3P_1$–$2s^22p\ 3d\ ^3D_2^\circ$	6.09E-01	6.02E-01	107.608	107.612(0.004)		2.151E+11	
2–42	$2s^22p^2\ ^3P_1$–$2s^22p\ 3d\ ^3D_1^\circ$	1.45E-01	1.48E-01		107.644		8.773E+10	
3–44	$2s^22p^2\ ^3P_2$–$2s^22p\ 3d\ ^3D_3^\circ$	1.00E+00	1.00E+00	107.683	107.684(0.001)		2.517E+11	
3–43	$2s^22p^2\ ^3P_2$–$2s^22p\ 3d\ ^3D_2^\circ$	9.17E-02	9.07E-02	107.742	107.747(0.005)		3.241E+10	
7–130	$2s\ 2p^3\ ^3D_3^\circ$–$2s\ 2p^2(^1D)3d\ ^3F_4$	1.58E-02	1.99E-02	108.555	108.545(−0.010)		1.822E+11	
2–37	$2s^22p^2\ ^3P_1$–$2s^22p\ 3d\ ^1D_2^\circ$	6.60E-03	8.12E-03	108.678	108.679(0.001)		1.208E+09	
3–36	$2s^22p^2\ ^3P_2$–$2s^22p\ 3d\ ^3F_3^\circ$	1.46E-01	1.71E-01		108.832		1.176E+09	
4–49	$2s^22p^2\ ^1D_2$–$2s^22p\ 3d\ ^1P_1^\circ$	5.18E-03	9.80E-03	109.763	109.775(0.012)		6.394E+09	
4–48	$2s^22p^2\ ^1D_2$–$2s^22p\ 3d\ ^1F_3^\circ$	6.45E-01	8.62E-01	109.896	109.905(0.009)		2.833E+11	
10–174	$2s\ 2p^3\ ^3P_2^\circ$–$2s\ 2p^2(^1D)3d\ ^3S_1$	1.81E-03	2.43E-03	110.750?	110.081(−0.669)		6.562E+10	
13–209	$2s\ 2p^3\ ^1D_2^\circ$–$2s\ 2p^2(^3P)3d\ ^1F_3$	8.84E-03	1.03E-02		110.742	110.750	2.154E+11	N
10–164	$2s\ 2p^3\ ^3P_2^\circ$–$2s\ 2p^2(^1D)3d\ ^3P_2$	3.66E-03	4.48E-03	112.448?	110.880(−1.568)		7.497E+10	
14–218	$2s\ 2p^3\ ^3S_1^\circ$–$2s^22p\ 5p\ ^3P_2$	1.82E-02	1.82E-02		111.004		2.752E+10	
14–217	$2s\ 2p^3\ ^3S_1^\circ$–$2s^22p\ 5p\ ^3P_1$	1.14E-02	1.13E-02		111.064		3.678E+10	
14–210	$2s\ 2p^3\ ^3S_1^\circ$–$2s^22p\ 5p\ ^1P_1$	2.97E-03	3.32E-03		111.732	111.725	5.827E+10	N
4–44	$2s^22p^2\ ^1D_2$–$2s^22p\ 3d\ ^3D_3^\circ$	1.33E-04	1.33E-04	111.725?	111.743(0.018)		3.469E+07	
14–207	$2s\ 2p^3\ ^3S_1^\circ$–$2s\ 2p^2(^3P)3d\ ^3P_2$	1.08E-02	1.07E-02		111.795	111.793	1.729E+11	N
4–43	$2s^22p^2\ ^1D_2$–$2s^22p\ 3d\ ^3D_2^\circ$	2.07E-04	2.05E-04	111.793?	111.811(0.018)		7.603E+07	
10–142	$2s\ 2p^3\ ^3P_2^\circ$–$2s\ 2p^2(^1D)3d\ ^3D_1$	2.76E-05	3.54E-05	112.009	112.019(0.010)		1.363E+09	
11–142	$2s\ 2p^3\ ^3P_1^\circ$–$2s\ 2p^2(^1D)3d\ ^3D_1$	4.87E-04	6.26E-04	112.009	112.019(0.010)		2.408E+10	
10–141	$2s\ 2p^3\ ^3P_2^\circ$–$2s\ 2p^2(^1D)3d\ ^3D_2$	4.70E-04	6.01E-04	112.009	112.021(0.012)		1.353E+10	
11–141	$2s\ 2p^3\ ^3P_1^\circ$–$2s\ 2p^2(^1D)3d\ ^3D_2$	1.64E-03	2.10E-03	112.009	112.021(0.012)		4.723E+10	
10–140	$2s\ 2p^3\ ^3P_2^\circ$–$2s\ 2p^2(^1D)3d\ ^3D_3$	3.15E-03	3.98E-03	112.009	112.022(0.013)		6.215E+10	
12–142	$2s\ 2p^3\ ^3P_0^\circ$–$2s\ 2p^2(^1D)3d\ ^3D_1$	7.00E-04	8.99E-04	112.009	112.026(0.017)		3.460E+10	
7–116	$2s\ 2p^3\ ^3D_3^\circ$–$2s\ 2p^2(^3P)3s\ ^3P_2$	1.93E-02	1.91E-02		112.182		1.004E+10	
14–205	$2s\ 2p^3\ ^3S_1^\circ$–$2s\ 2p^2(^3P)4s\ ^3P_2$	8.16E-03	8.29E-03		112.566		6.956E+09	
4–37	$2s^22p^2\ ^1D_2$–$2s^22p\ 3d\ ^1D_2^\circ$	3.07E-01	3.77E-01	112.950	112.963(0.013)		5.839E+10	
4–35	$2s^22p^2\ ^1D_2$–$2s^22p\ 3d\ ^3F_2^\circ$	1.83E-01	2.18E-01	113.125	113.139(0.014)		4.000E+10	
5–49	$2s^22p^2\ ^1S_0$–$2s^22p\ 3d\ ^1P_1^\circ$	1.31E-01	2.48E-01	114.666	114.687(0.021)		1.688E+11	
15–215	$2s\ 2p^3\ ^1P_1^\circ$–$2s^22p\ 5p\ ^1D_2$	9.79E-03	1.25E-02		115.148		2.115E+10	
7–94	$2s2p^3\ ^3D_3^\circ$–$2s\ 2p^2(^3P)3d\ ^3D_3$	1.48E-02	1.57E-02	115.729	115.740(0.011)		4.040E+10	
8–93	$2s2p^3\ ^3D_2^\circ$–$2s\ 2p^2(^3P)3d\ ^3D_2$	7.51E-03	8.07E-03	115.780	115.790(0.010)		2.880E+10	
10–116	$2s2p^3\ ^3P_2^\circ$–$2s\ 2p^2(^3P)3s\ ^3P_2$	1.20E-02	1.18E-02		117.080		6.514E+09	
7–91	$2s2p^3\ ^3D_3^\circ$–$2s\ 2p^2(^3P)3d\ ^3F_4$	6.70E-02	7.43E-02	117.491	117.503(0.012)		1.034E+11	
8–90	$2s2p^3\ ^3D_2^\circ$–$2s\ 2p^2(^3P)3d\ ^3F_3$	4.75E-02	5.23E-02	117.609	117.624(0.015)		9.232E+10	
9–89	$2s2p^3\ ^3D_1^\circ$–$2s\ 2p^2(^3P)3d\ ^3F_2$	3.17E-02	3.56E-02	117.699	117.711(0.012)		8.686E+10	
15–187	$2s2p^3\ ^1P_1^\circ$–$2s\ 2p^2(^1S)3d\ ^1D_2$	2.81E-03	6.65E-03		117.873		1.577E+10	
8–87	$2s2p^3\ ^3D_2^\circ$–$2s\ 2p^2(^3P)3d\ ^3P_1$	2.18E-03	2.60E-03	118.500	118.517(0.017)		7.909E+09	
7–86	$2s2p^3\ ^3D_3^\circ$–$2s\ 2p^2(^3P)3d\ ^3P_2$	4.64E-03	5.60E-03	118.585	118.600(0.015)		1.011E+10	
13–175	$2s2p^3\ ^1D_2^\circ$–$2s\ 2p^2(^1D)3d\ ^1P_1$	5.36E-03	7.35E-03	119.204	119.206(0.002)		4.623E+10	
8–80	$2s2p^3\ ^3D_2^\circ$–$2s\ 2p^2(^3P)3d\ ^5D_2$	3.99E-06	5.52E-06	119.415?	119.669(0.254)		9.476E+05	
13–173	$2s2p^3\ ^1D_2^\circ$–$2s\ 2p^2(^1D)3d\ ^1D_2$	1.28E-02	1.81E-02	119.684	119.692(0.008)		1.173E+11	
13–165	$2s2p^3\ ^1D_2^\circ$–$2s^22p\ 4f\ ^1F_3$	8.09E-03	1.04E-02		120.323		3.714E+10	
13–164	$2s2p^3\ ^1D_2^\circ$–$2s\ 2p^2(^1D)3d\ ^3P_2$	7.53E-07	9.18E-07	122.199?	120.363(−1.836)		1.670E+07	
14–175	$2s2p^3\ ^3S_1^\circ$–$2s\ 2p^2(^1D)3d\ ^1P_1$	8.74E-06	1.20E-05	120.355	120.384(0.029)		7.597E+07	
10–94	$2s2p^3\ ^3P_2^\circ$–$2s\ 2p^2(^3P)3d\ ^3D_3$	3.05E-02	3.22E-02	120.931	120.960(0.029)		8.689E+10	
11–93	$2s2p^3\ ^3P_1^\circ$–$2s\ 2p^2(^3P)3d\ ^3D_2$	1.58E-02	1.70E-02	120.973	121.002(0.029)		6.320E+10	
12–92	$2s2p^3\ ^3P_0^\circ$–$2s\ 2p^2(^3P)3d\ ^3D_1$	7.27E-03	7.67E-03	121.004	121.036(0.032)		4.739E+10	
6–41	$2s2p^3\ ^5S_2^\circ$–$2s\ 2p^2(^3P)3s\ ^5P_3$	2.27E-01	4.06E-01	121.773	121.781(0.008)		2.509E+10	
6–40	$2s2p^3\ ^5S_2^\circ$–$2s\ 2p^2(^3P)3s\ ^5P_2$	1.60E-01	2.79E-01	121.913	121.921(0.008)		2.500E+10	
6–39	$2s2p^3\ ^5S_2^\circ$–$2s\ 2p^2(^3P)3s\ ^5P_1$	9.70E-02	1.70E-01	122.018	122.025(0.007)		2.492E+10	
13–134	$2s2p^3\ ^1D_2^\circ$–$2s\ 2p^2(^1D)3d\ ^1F_3$	2.09E-02	2.75E-02		122.266		2.210E+10	
7–69	$2s2p^3\ ^3D_3^\circ$–$2s\ 2p^2(^1D)3s\ ^3D_3$	3.10E-02	3.80E-02	123.134	123.140(0.006)		3.046E+10	
2–23	$2s^22p^2\ ^3P_1$–$2s^22p\ 3s\ ^3P_2^\circ$	2.46E-01	2.71E-01	123.744	123.770(0.026)		8.027E+09	
1–22	$2s^22p^2\ ^3P_0$–$2s^22p\ 3s\ ^3P_1^\circ$	1.91E-01	2.10E-01	123.868	123.893(0.025)		1.061E+10	
3–23	$2s^22p^2\ ^3P_2$–$2s^22p\ 3s\ ^3P_2^\circ$	7.35E-01	8.08E-01	123.929	123.948(0.019)		2.402E+10	
2–22	$2s^22p^2\ ^3P_1$–$2s^22p\ 3s\ ^3P_1^\circ$	1.42E-01	1.57E-01	123.970	123.999(0.029)		7.899E+09	

Table 5
(Continued)

i–j	Transition	Int (10^9)	Int (10^{13})	$\lambda_{\rm NIST}$	$\lambda_{\rm MCDHF}$	$\lambda_{\rm rev}$	$A_{\rm MCDHF}$	Note
13–125	$2s2p^3\ ^1D_2°$–$2s^22p\ 4p\ ^1D_2$	1.09E-02	1.42E-02		124.059		1.081E+09	
11–86	$2s2p^3\ ^3P_1°$–$2s\ 2p^2(^3P)3d\ ^3P_2$	8.10E-03	9.77E-03		124.088		1.846E+10	
10–86	$2s2p^3\ ^3P_2°$–$2s\ 2p^2(^3P)3d\ ^3P_2$	2.08E-02	2.51E-02	124.059	124.088(0.029)		4.748E+10	
2–21	$2s^22p^2\ ^3P_1$–$2s^22p\ 3s\ ^3P_0°$	1.80E-01	1.97E-01		124.090		3.196E+10	
3–22	$2s^22p^2\ ^3P_2$–$2s^22p\ 3s\ ^3P_1°$	2.39E-01	2.64E-01	124.153	124.178(0.025)		1.334E+10	
13–122	$2s2p^3\ ^1D_2°$–$2s^22p\ 4p\ ^3P_1$	1.39E-02	1.41E-02		124.698		7.140E+09	
15–175	$2s2p^3\ ^1P_1°$–$2s\ 2p^2(^1D)3d\ ^1P_1$	3.60E-03	4.93E-03	124.850	124.881(0.031)		3.246E+10	
15–173	$2s2p^3\ ^1P_1°$–$2s\ 2p^2(^1D)3d\ ^1D_2$	3.78E-03	5.36E-03	125.383	125.415(0.032)		3.634E+10	
14–124	$2s2p^3\ ^3S_1°$–$2s^22p\ 4p\ ^3P_2$	1.71E-02	1.75E-02		125.880		1.350E+09	
4–24	$2s^22p^2\ ^1D_2$–$2s^22p\ 3s\ ^1P_1°$	5.00E-01	6.50E-01	127.837	127.870(0.033)		3.797E+10	
14–116	$2s2p^3\ ^3S_1°$–$2s\ 2p^2(^3P)3s\ ^3P_2$	2.29E-02	2.27E-02		129.057		1.373E+10	
10–69	$2s2p^3\ ^3P_2°$–$2s\ 2p^2(^1D)3s\ ^3D_3$	1.17E-02	1.44E-02	129.040	129.067(0.027)		1.208E+10	
7–52	$2s2p^3\ ^3D_3°$–$2s\ 2p^2(^3P)3s\ ^3P_2$	1.91E-01	1.92E-01	133.825	133.846(0.021)		1.848E+10	
8–52	$2s2p^3\ ^3D_2°$–$2s\ 2p^2(^3P)3s\ ^3P_2$	2.88E-02	2.90E-02		133.863		2.788E+09	
8–51	$2s2p^3\ ^3D_2°$–$2s\ 2p^2(^3P)3s\ ^3P_1$	1.09E-01	1.08E-01	134.021	134.049(0.028)		1.706E+10	
9–51	$2s2p^3\ ^3D_1°$–$2s\ 2p^2(^3P)3s\ ^3P_1$	3.26E-02	3.23E-02		134.056		5.119E+09	
9–50	$2s2p^3\ ^3D_1°$–$2s\ 2p^2(^3P)3s\ ^3P_0$	4.53E-02	4.75E-02	134.135	134.160(0.025)		2.254E+10	
5–24	$2s^22p^2\ ^1S_0$–$2s^22p\ 3s\ ^1P_1°$	1.45E-01	1.89E-01	134.532	134.585(0.053)		1.162E+10	
15–108	$2s2p^3\ ^1P_1°$–$2s\ 2p^2(^1S)3s\ ^1S_0$	6.12E-03	1.52E-02		135.181		2.724E+10	
14–86	$2s2p^3\ ^3S_1°$–$2s\ 2p^2(^3P)3d\ ^3P_2$	4.54E-03	5.48E-03	137.589	137.625(0.036)		1.148E+10	
13–77	$2s2p^3\ ^1D_2°$–$2s\ 2p^2(^1D)3s\ ^1D_2$	1.09E-01	1.51E-01	138.693	138.722(0.029)		1.579E+10	
10–52	$2s2p^3\ ^3P_2°$–$2s\ 2p^2(^3P)3s\ ^3P_2$	1.24E-01	1.24E-01	140.833	140.878(0.045)		1.257E+10	
11–52	$2s2p^3\ ^3P_1°$–$2s\ 2p^2(^3P)3s\ ^3P_2$	4.13E-02	4.15E-02		140.878		4.204E+09	
10–51	$2s2p^3\ ^3P_2°$–$2s\ 2p^2(^3P)3s\ ^3P_1$	3.82E-02	3.78E-02	141.040	141.084(0.044)		6.303E+09	
11–51	$2s2p^3\ ^3P_1°$–$2s\ 2p^2(^3P)3s\ ^3P_1$	2.55E-02	2.52E-02		141.084		4.202E+09	
12–51	$2s2p^3\ ^3P_0°$–$2s\ 2p^2(^3P)3s\ ^3P_1$	3.31E-02	3.27E-02		141.095		5.467E+09	
11–50	$2s2p^3\ ^3P_1°$–$2s\ 2p^2(^3P)3s\ ^3P_0$	2.97E-02	3.12E-02		141.200		1.555E+10	
15–77	$2s2p^3\ ^1P_1°$–$2s\ 2p^2(^1D)3s\ ^1D_2$	2.78E-02	3.84E-02	146.398	146.468(0.070)		4.236E+09	
7–32	$2s2p^3\ ^3D_3°$–$2s^22p\ 3p\ ^3P_2$	3.27E-01	3.38E-01	149.442	149.478(0.036)		3.012E+09	
8–32	$2s2p^3\ ^3D_2°$–$2s^22p\ 3p\ ^3P_2$	5.95E-02	6.14E-02		149.499		5.478E+08	
8–31	$2s2p^3\ ^3D_2°$–$2s^22p\ 3p\ ^3P_1$	1.72E-01	1.77E-01	149.621	149.658(0.037)		2.663E+09	
9–31	$2s2p^3\ ^3D_1°$–$2s^22p\ 3p\ ^3P_1$	5.82E-02	5.98E-02		149.667		8.994E+08	
9–30	$2s2p^3\ ^3D_1°$–$2s^22p\ 3p\ ^3P_0$	7.39E-02	7.83E-02		149.794		3.668E+09	

Note. Using the present atomic data (wavelengths $\lambda_{\rm MCDHF}$ (in angstroms) and transition rates $A_{\rm MCDHF}$ (in s^{-1})) and electron-impact excitation data provided by Mao et al. (2020), relative intensities (photons) $Int = N_j A_{ji}/N_e$ are calculated at a fixed temperature T_e [K] $= 4 \times 10^5$, and at low and high electron densities N_e [cm^{-3}] $= 10^9$ (column 3) and 10^{13} (column 4), typical of the quiet solar corona and of laboratory spectra. Relative intensities are normalized to the intensity of the brightest line for the transition $\#3/2s^22p^2\ ^3P_2$–$\#44/2s^22p\ 3d\ ^3D_3°$. The lines are displayed in increasing order of the present wavelengths $\lambda_{\rm MCDHF}$. $\lambda_{\rm NIST}$: experimental wavelengths (in angstroms) observed by Söderqvist (1946), which are listed in the NIST database; $\lambda_{\rm MCDHF}$: the present wavelengths (with the difference with the experimental value in brackets); $A_{\rm MCDHF}$: the present transition rates; $\lambda_{\rm rev}$: new experimental wavelengths that we propose. A question mark in column $\lambda_{\rm NIST}$ indicates that its identification is questionable. The symbol N in the last column "Note" means that a tentative assignment is provided.

(This table is available in its entirety in machine-readable form.)

Söderqvist (1946) assigned the $2s\,2p^3\ ^5S_2°$–$2s\,2p^2(^3P)3d\ ^5D_3$ transition between states #6 and #180 to a line at 106.580 Å. However, this wavelength differs from our MCDHF result (106.701 Å) by −0.121 Å so we reject this identification. This line at 106.580 Å is close to the MCDHF result ($\lambda_{\rm MCDHF} =$ 106.599 Å) for the transition $\#8/2s\,2p^3\ ^3D_2°$–$\#160/2s^2\,2p\,4f\ ^1D_2$ to within 0.019 Å. Therefore, we tentatively assign the observed line 106.580 Å to the latter transition #8–#160, though its intensity is not very strong. Using this new identification at 106.580 Å and the experimental excitation energy 204,223 cm^{-1} for the lower state $\#8/2s\,2p^3\ ^3D_2°$, the experimental value for the upper level $\#160/2s^2\,2p\,4f\ ^1D_2$ then should be 114,2485 cm^{-1}. This new excitation energy again shows good agreement (within 70 cm^{-1}) with our MCDHF computed excitation energy of 1,142,424 cm^{-1}.

As shown in Table 5, the $2s^22p4p$ states produce three strong transitions in the EUV wavelength range from 124 to 126 Å. In the same wavelength range, the $3d \rightarrow 2p$ transitions with similar or lower intensities have been observed by Söderqvist (1946). The present accurate transition wavelengths $\lambda_{\rm MCDHF}$ involving the $2s^22p4p$ states would aid the spectral analysis of a future experiment.

The $2s^22p4s$ and $2s2p^24s$ states produce measurable transitions (with the relative intensity from 10^{-3} to 10^{-2}) in the X-ray range. Tentative identifications involving the $2s^22p4s$ and $2s2p^24s$ configurations by Söderqvist (1946) at 90.746 Å, 91.737 Å, 91.836 Å, and 99.004 Å, differ from our MCDHF results (90.830 Å, 91.373 Å, 91.470 Å, and 99.510 Å) by 0.084 Å, −0.364 Å, −0.366 Å, and 0.506 Å, respectively. Another two transitions from the $2s2p^24s$ states with the relative intensity around 10^{-2}, associated with the MCDHF wavelengths ($\lambda_{\rm MCDHF} =$ 103.345 and 112.566 Å), have not yet been observed. Clearly, further studies, supported by more detailed laboratory observations, are needed to sort out the identifications involving these two configurations $2s^2 2p4s$ and $2s2p^2 4s$.

3.2.3. The n = 3 → n = 2 Lines

The strongest line at both low and high plasma densities arises from the $2s^2\,2p^2\ ^3P_2$–$2s^2\,2p\,3d\ ^3D_3^\circ$ transition between states #3 and #44, and was identified at 107.683 Å by Söderqvist (1946). The corresponding theoretical MCDHF wavelength is 107.684 Å, and good agreement (within 0.001 Å) is found between experimental and theoretical wavelengths. On the basis of our MCDHF calculations, Table 5 implies that almost all identifications (another 15 lines) of the $2s^2 2p3d \rightarrow 2s^2 2p^2$ transition array suggested by Söderqvist (1946) in the EUV range (from 107 Å to 115 Å) are correct.

Two exceptions are the lines at 111.725 and 111.793 Å, which were tentatively assigned to incorrect transitions $\#4/2s^2\,2p^2\ ^1D_2$–$\#44/2s^2\,2p\,3d\ ^3D_3^\circ$ and $\#4/2s^2\,2p^2\ ^1D_2$–$\#43/2s^2\,2p\,3d\ ^3D_2^\circ$, respectively. The line at 111.725 Å has been discussed above in Section 3.2.1.

Söderqvist (1946) assigned the line at 111.793 Å to the transition $\#4/2s^2\,2p^2\ ^1D_2$–$\#43/2s^2\,2p\,3d\ ^3D_2^\circ$. As shown in Table 5, the predicted intensities of this transition #4–#43 are relatively low at both low and high plasma densities. By contrast, the relative intensity of the $2s\,2p^3\ ^3S_1^\circ$–$2s\,2p^2(^3P)3d\ ^3P_2$ transition (#14–#207) is almost two orders of magnitude larger than the intensity of the former transition (#4–#43). Considering that the line at 111.793 Å is also in good agreement with our MCDHF wavelength $\lambda_{\rm MCDHF} = 111.795$ Å for the latter transition, we suggest assigning this line 111.793 Å to the transition $\#14/2s\,2p^3\ ^3S_1^\circ$–$\#207/2s\,2p^2(^3P)3d\ ^3P_2$. Then, the experimental value for the upper level $\#207/2s\,2p^2(^3P)3d\ ^3P_2$ is 1,215,099 cm^{-1}, and shows good agreement (within 190 cm^{-1}) with our MCDHF computed excitation energy of 1,215, 284 cm^{-1}.

Söderqvist (1946) identified many transitions of the $2s2p^2 3d \rightarrow 2s3p^3$ array, and the excitation energies were included in the NIST database. At both low and high plasma densities, the strongest identified lines at 117.491 and 117.609 Å are the transitions $\#7/2s\,2p^3\ ^3D_3^\circ$–$\#91/2s\,2p^2(^3P)3d\ ^3F_4$ and $\#8/2s\,2p^3\ ^3D_2^\circ$–$\#90/2s\,2p^2(^3P)3d\ ^3F_3$, respectively. These two wavelengths are in good agreement with the present MCDHF values (117.503 Å and 117.624 Å), so the identifications are confirmed.

On the basis of our MCDHF calculations, almost all identifications (another 24 lines) suggested by Söderqvist (1946) in the EUV range (from 106 Å to 138 Å) are listed in Table 5, which come from the $2s2p^2 3d \rightarrow 2s3p^3$ transition array, and are also correct.

The line at 106.580 Å was assigned to incorrect transitions $\#6/2s\,2p^3\ ^5S_2^\circ$–$\#81/2s\,2p^2(^3P)3d\ ^5D_3$, and has been discussed above in Section 3.2.2. Söderqvist (1946) assigned the line at 110.750 Å to the transition $\#10/2s\,2p^3\ ^3P_2^\circ$–$\#174/2s\,2p^2(^1D)3d\ ^3S_1$. As shown in Table 5, the predicted intensities of this transition #10–#174 at both low and high plasma densities are much smaller than the intensities of the transition (#13–#209) belonging to the same array $2s2p^2 3d \rightarrow 2s3p^3$, associated with the present MCDHF value ($\lambda_{\rm MCDHF} =$ 110.742 Å). Hence, we suggest to assign the line 110.750 Å to the transition $\#13/2s\,2p^3\ ^1D_2^\circ$–$\#209/2s\,2p^2(^3P)3d\ ^1F_3$. The experimental value for the upper level #209 is then 1,215,250 cm^{-1}, which shows excellent agreement (within 40 cm^{-1}) with our MCDHF computed excitation energy of 1,215,284 cm^{-1}.

The line at 107.535 Å included in the NIST database was incorrectly assigned by Söderqvist (1946) to the transition $\#7/2s\,2p^3\ ^3D_3^\circ$–$\#142/2s\,2p^2(^1D)3d\ ^3D_1$, since this transition with $\Delta J = 2$ is predicted to be too weak to be observed. This observed wavelength is close to the MCDHF value (107.530 Å) associated with the $\#7/2s\,2p^3\ ^3D_3^\circ$–$\#140/2s\,2p^2(^1D)3d\ ^3D_3$ transition. The predicted relative intensities for the latter transition (#7–#140) are such that they should be visible at both low and high plasma densities. Hence, we suggest assigning the line at 107.535 Å to the transition #7–#140.

There are the four lines at 107.934 Å, 112.448 Å, 119.415 Å, and 122.199 Å belonging to the transition array $2s2p^2 3d \rightarrow 2s3p^3$ listed in Table 5, for which we cannot find any obvious counterparts in the present calculated MCDHF wavelengths, and misidentifications for these lines cannot be ruled out. For example, it can be seen from Table 5 that the transitions #8–#80 and #13–#164, assigned to the lines 119.415 Å and 122.199 Å, respectively, are too weak to be observed at either low or high plasma densities.

The $2s^2 2p3p$ states produce five strong transitions around 149 Å. Two lines at 149.442 Å and 149.621 Å, respectively, assigned to the transitions $\#7/2s\,2p^3\ ^3D_3^\circ$–$\#32/2s^2\,2p\,3p\ ^3P_2$ and $\#8/2s\,2p^3\ ^3D_2^\circ$–$\#31/2s^2\,2p\,3p\ ^3P_1$ were identified by Söderqvist (1946). These two lines agree well with our MCDHF values $\lambda_{\rm MCDHF}$ of 149.478 Å and 149.658 Å, respectively.

For the strongest lines (#1–#67, #2–#68, #3–#68, #3–#67, #2–#63, #3–#64, #3–#63, #1–#53, #2–#53, and #3–#53) of the $2s2p^2 3p \rightarrow 2s^2 2p^2$ transition array listed in Table 5, a good agreement (within 0.027 Å) of the present MCDHF wavelengths and the experiment results reported by Söderqvist (1946) is found.

The identifications of two lines at 95.933 and 96.475 Å were incorrectly assigned by Söderqvist (1946) to the transitions $\#4/2s^2\,2p^2\ ^1D_2$–$\#98/2s\,2p^2(^1D)3p\ ^1D_2^\circ$ and $\#4/2s^2\,2p^2\ ^1D_2$–$\#100/2s\,2p^2(^1D)3p\ ^1F_3^\circ$, respectively. The identifications of these two lines should be exchanged with each other, since the lines at 95.933 and 96.475 Å show good agreement with our MCDHF values $\lambda_{\rm MCDHF}$ of 95.928 Å for the transition #4–#100 and 96.473 Å the transition #4–#98, respectively. However, the lines at 96.124 Å 96.196 Å and 96.307 Å listed in the NIST database, respectively, tentatively assigned by Söderqvist (1946) to the transitions $\#1/2s^2\,2p^2\ ^3P_0$–$\#101/2s\,2p^2(^1D)3p\ ^3D_1^\circ$, $\#2/2s^2\,2p^2\ ^3P_1$–$\#101/2s\,2p^2(^1D)3p\ ^3D_1^\circ$, and $\#3/2s^2\,2p^2\ ^3P_2$–$\#103/2s\,2p^2(^1D)3p\ ^3D_3^\circ$ show a large difference of about 3.4 Å with our MCDHF wavelengths, $\lambda_{\rm MCDHF} = 92.695$ Å, 92.755 Å, and 92.846 Å.

The identifications of another 19 lines involving the upper states of the $2s^2 2p3s$ and $2s2p^2 3s$ configurations in the wavelength range between 121 and 147 Å are confirmed by our theoretical MCDHF calculations since a good agreement is found between experimental and theoretical wavelengths.

3.3. Transition Rates and Lifetimes

The accuracy of the present MCDHF radiative transition data is evaluated by comparing two sets of line strengths $S_l\,(\mathrm{AS}_4)$ and $S_l\,(\mathrm{AS}_5)$ in the length form obtained from calculations based on the AS_4 and AS_5 active sets, as well as by comparing two sets of line strengths $S_l\,(\mathrm{AS}_5)$ in the length form and

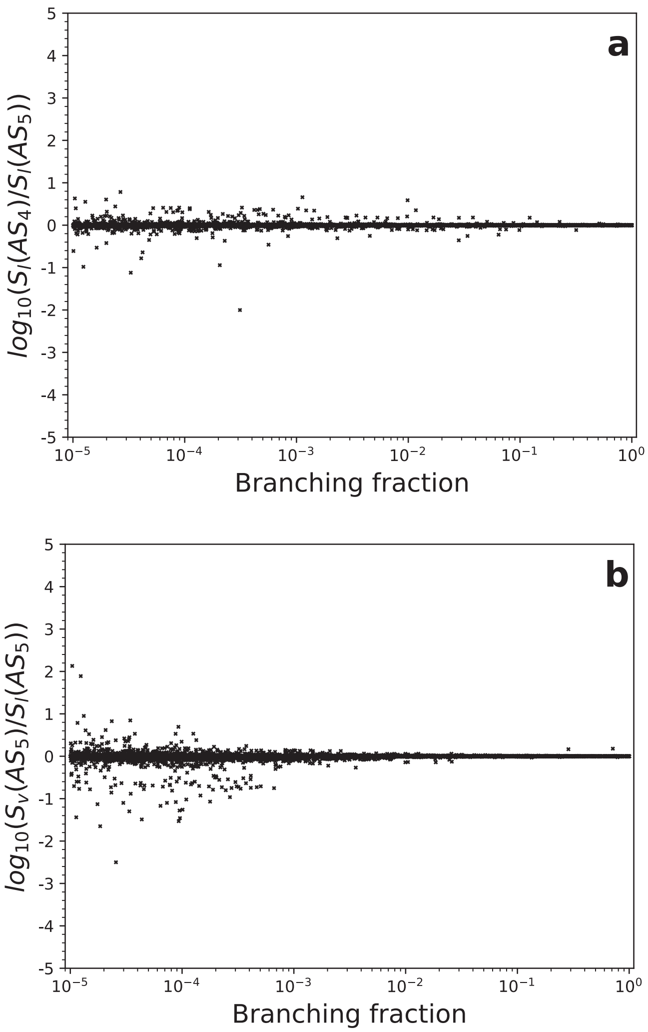

Figure 2. (a) $\log_{10}(S_l\,(AS_4)/S_l\,(AS_5))$ vs. branching fraction for all E1 transitions of Na VI included in Table 3. (b) $\log_{10}(S_v\,(AS_5)/S_l\,(AS_5))$ vs. branching fraction for all E1 transitions of Na VI included in Table 3.

$S_v\,(AS_5)$ in the velocity form obtained from calculations based on the AS_5 active set. As an example, the logarithm of the ratio between line strengths $S_l\,(AS_4)$ and $S_l\,(AS_5)$, given in Table 3, is plotted in Figure 2(a) versus branching fraction (BF) for all E1 transitions of Na VI listed in Table 3. Good agreement between line strengths $S_l\,(AS_4)$ and $S_l\,(AS_5)$ is obtained for most of E1 transitions in Na VI. A regular distribution of points with scatter rapidly decreasing with increasing BF values is observed. As shown in Figure 2(b), a similar phenomenon can be found in the comparison between line strengths $S_v\,(AS_5)$ and $S_l\,(AS_5)$.

By comparing two sets of line strengths $S_l\,(AS_4)$ and $S_l\,(AS_5)$ in the length form obtained from the present MCDHF calculations of the AS_4 and AS_5 active sets, the uncertainty estimation method, provided by Kramida (2013, 2014), is used to classify the accuracy of the present MCDHF radiative transition data, according to the NIST database (Kramida et al. 2020) terminology (AA $\leqslant$1%, A$^+$ $\leqslant$2%, A $\leqslant$3%, B$^+$ $\leqslant$7%, B $\leqslant$10%, C$^+$ $\leqslant$18%, C $\leqslant$25%, D$^+$ $\leqslant$40%, D $\leqslant$50%, and E > 50%). Defining the difference δS between two sets of line strengths ($S_l\,(AS_4)$ and $S_l\,(AS_5)$) as $\delta S = |S_l\,(AS_4)-S_l\,(AS_5)|/\max(S_l\,(AS_4),\, S_l\,(AS_5))$, the averaged uncertainties δS_{av} for line strengths S of E1 transitions in various ranges of S in Na VI are assessed to 1.2% for $S \geqslant 10^0$, 2.0% for $10^0 > S \geqslant 10^{-1}$, 3.0% for $10^{-1} > S \geqslant 10^{-2}$, 4.2% for $10^{-2} > S \geqslant 10^{-3}$, 5.3% for $10^{-3} > S \geqslant 10^{-4}$, 5.6% for $10^{-4} > S \geqslant 10^{-5}$, 6.1% for $10^{-5} > S \geqslant 10^{-6}$, and 8.0% for $10^{-6} > S \geqslant 10^{-7}$. Then, $\max(\delta S_{ji},\, \delta S_{av})$ is accepted as the uncertainty of each particular line strength S_{ji}. In Table 3, about 8.5% of E1 S values in Na VI have uncertainties of $\leqslant$2% (A+), 38.6% have uncertainties of $\leqslant$3% (A), 43.4% have uncertainties of $\leqslant$7% (B+), 3.2% have uncertainties of $\leqslant$10% (B), 2.9% have uncertainties of $\leqslant$18% (C+), 1.1% have uncertainties of $\leqslant$25% (C), and 1.2% have uncertainties of $\leqslant$40% (D+), while only 1.2% have uncertainties of >40% (D and E).

The uncertainties of line strengths S for E2, M1, and M2 transitions in Na VI are estimated using the same ranking method, as well as those for E1, E2, M1, and M2 transitions in O III, F IV, Ne V, and Mg VII. In Table 3, the estimated uncertainties for all E1 M1, E2, and M2 transitions with BF $\geqslant 10^{-5}$ in O III, F IV, Ne V, Na VI, and Mg VII are provided. It should be noted that the uncertainty of the S value for each transition is estimated by including all transitions (without a restriction of BF values) of a single ion in the uncertainty estimation procedure, though only transitions with BF $\geqslant 10^{-5}$ are provided in Table 3.

Radiative lifetimes ($\tau^l_{\rm MCDHF}$ in the length form and $\tau^v_{\rm MCDHF}$ in the velocity form) from the present MCDHF calculations based on AS_5 active set are provided in Table 2 for the 156 (196, 215, 272, 318) lowest states of the $2s^22p^2$, $2s2p^3$, $2p^4$, $2s^22p3s$, $2s^22p3p$, $2s^22p3d$, $2s2p^23s$, $2s2p^23p$, $2s2p^23d$, $2p^33s$, $2p^33p$, $2p^33d$, $2s^22p4s$, $2s^22p4p$, $2s^22p4d$, $2s^22p4f$, $2s2p^24s$, $2s2p^24p$, $2s2p^24d$, $2s2p^24f$, $2s^22p5s$, $2s^22p5p$, $2s^22p5d$, $2s^22p5f$, and $2s^22p5g$ configurations in O III (F IV, Ne V, Na VI, Mg VII), which are calculated by including all possible E1, E2, M1, and M2 radiative transition rates. The present MCDHF radiative lifetimes $\tau^l_{\rm MCDHF}$ and $\tau^v_{\rm MCDHF}$ show good agreement, within a difference of 1% for most states of all five ions.

Comparisons with previous theoretical and experimental lifetimes were provided in Table 6. Previous theoretical lifetimes from the MCDHF1 calculations by Jönsson & Bieroń (2010); Jönsson et al. (2011) and the MCHF calculations by Tachiev & Froese Fischer (2001), Froese Fischer & Tachiev (2004) show good agreement with the present MCDHF lifetimes. The differences are generally within 5% except for the level #23/$2s^2\,2p\,3p$ $^1P_1$ of O III with a difference of 7%.

The lifetimes for the levels #5/$2s^2\,2p^2$ $^1S_0$ with $Z = 8-10$ and the level #6/$2s\,2p^3$ $^5S_2^\circ$ of F IV were measured accurately using a heavy-ion storage ring (Träbert et al. 2000, 2012) as an electron source. Using an electron cyclotron ion source, Smith et al. (2004) also accurately provided the lifetimes for the level #5/$2s^2\,2p^2$ $^1S_0$ of O III. Our computed MCDHF lifetimes, as well as the MCDHF1 and MCHF values, are in good agreement with these measurements. The experimental lifetime of the level #6/$2s\,2p^3$ $^5S_2^\circ$ of F IV, determined from the direct measurement of the time dependence of spontaneous emission of O^{+2} ions (Johnson et al. 1984), is also in good agreement with our MCDHF lifetime.

The remaining experimental lifetimes for the $n = 2$ levels from O III to Mg VII and the $n = 3$ levels of O III are from relatively early beam-foil measurements in the 1970s and 1980s. Some measurements show a relatively large difference of $\geqslant$ 10% with all the calculated values (MCDHF, MCDHF1, and MCHF). As an example, the experimental lifetimes and the present MCDHF values for the $2s\,2p^3$ $^3D_2^\circ$ and $2s\,2p^3$ $^3P_2^\circ$

Table 6
Comparisons between the Experimental and Theoretical Lifetimes (in seconds) for the $n \leqslant 3$ States of the Ion from O III to Mg VII

Z	Key	State	Experiment[a]	Uncertainty[a]	MCDHF[b]	MCDHF1[c]	MCHF[d]
8	5	$2s^22p^2\ ^1S_0$	5.30E-1 [e]	0.25E-01	5.152E-01	⋯	5.234E-01
8	5	$2s^22p^2\ ^1S_0$	5.40E-01 [f]	0.27E-01	5.152E-01	⋯	5.234E-01
9	5	$2s^22p^2\ ^1S_0$	3.04E-01 [e]	0.05E-01	2.953E-01	2.952E-01	3.003E-01
10	5	$2s^22p^2\ ^1S_0$	1.28E-01 [g]	0.16E-01	1.417E-01	1.418E-01	1.434E-01
8	6	$2s2p^3\ ^5S_2^\circ$	1.250E-03 [e]	0.013E-03	1.288E-03	⋯	1.237E-03
8	6	$2s2p^3\ ^5S_2^\circ$	1.22E-03 [h]	0.08E-03	1.288E-03	⋯	1.237E-03
8	8	$2s2p^3\ ^3D_2^\circ$	1.61E-09 [i]	0.07E-09	1.610E-09	1.610E-09	1.602E-09
9	8	$2s2p^3\ ^3D_2^\circ$	1.21E-09 [j]	0.07E-09	1.140E-09	1.143E-09	1.131E-09
10	8	$2s2p^3\ ^3D_2^\circ$	**1.076E-09** [k]	0.030E-09	8.740E-10	8.753E-10	8.590E-10
11	8	$2s2p^3\ ^3D_2^\circ$	7.5E-10 [l]	0.8E-10	7.028E-10	7.029E-10	6.805E-10
12	8	$2s2p^3\ ^3D_2^\circ$	**6.94E-10** [k]	0.14E-10	5.832E-10	5.832E-10	5.637E-10
8	10	$2s2p^3\ ^3P_2^\circ$	5.75E-10 [i]	0.18E-10	5.416E-10	5.435E-10	5.382E-10
9	10	$2s2p^3\ ^3P_2^\circ$	4.3E-10 [j]	0.3E-10	4.048E-10	4.066E-10	4.011E-10
10	10	$2s2p^3\ ^3P_2^\circ$	**3.80E-10** [k]	0.13E-10	3.175E-10	3.214E-10	3.153E-10
11	10	$2s2p^3\ ^3P_2^\circ$	2.8E-10 [l]	0.3E-10	2.639E-10	2.642E-10	2.565E-10
12	11	$2s2p^3\ ^3P_2^\circ$	2.44E-10 [k]	0.24E-10	2.234E-10	2.197E-10	2.169E-10
8	13	$2s2p^3\ ^1D_2^\circ$	2.0E-10 [i]	0.5E-10	1.828E-10	1.825E-10	1.813E-10
9	13	$2s2p^3\ ^1D_2^\circ$	**1.55E-10** [j]	0.15E-10	1.331E-10	1.327E-10	1.319E-10
10	13	$2s2p^3\ ^1D_2^\circ$	**1.44E-10** [k]	0.14E-10	1.051E-10	1.050E-10	1.035E-10
11	13	$2s2p^3\ ^1D_2^\circ$	**1.05E-10** [l]	0.15E-10	8.687E-11	8.675E-11	8.462E-11
12	13	$2s2p^3\ ^1D_2^\circ$	**8.8E-11** [k]	0.3E-11	7.385E-11	7.377E-11	7.186E-11
8	14	$2s2p^3\ ^3S_1^\circ$	**7.9E-11** [i]	0.4E-11	6.966E-11	6.983E-11	6.939E-11
9	14	$2s2p^3\ ^3S_1^\circ$	⋯	⋯	5.580E-11	5.584E-11	5.542E-11
10	14	$2s2p^3\ ^3S_1^\circ$	**6.1E-11** [k]	0.4E-11	4.645E-11	4.646E-11	4.585E-11
11	14	$2s2p^3\ ^3S_1^\circ$	**4.8E-11** [l]	0.5E-11	3.971E-11	3.969E-11	3.881E-11
12	14	$2s2p^3\ ^3S_1^\circ$	**4.5E-11** [k]	0.4E-11	3.459E-11	3.457E-11	3.376E-11
8	15	$2s2p^3\ ^1P_1^\circ$	8.7E-11 [i]	0.6E-11	9.140E-11	9.233E-11	9.091E-11
9	15	$2s2p^3\ ^1P_1^\circ$	7.2E-11 [j]	1.1E-11	7.377E-11	7.410E-11	7.314E-11
10	15	$2s2p^3\ ^1P_1^\circ$	**8.9E-11** [k]	0.3E-11	6.097E-11	6.109E-11	6.007E-11
11	15	$2s2p^3\ ^1P_1^\circ$	5.5E-11 [l]	0.6E-11	5.169E-11	5.170E-11	5.043E-11
12	15	$2s2p^3\ ^1P_1^\circ$	**5.0E-11** [k]	0.3E-11	4.468E-11	4.469E-11	4.357E-11
8	16	$2s^22p\ 3s\ ^3P_0^\circ$	2.66E-10 [m]	0.11E-10	2.539E-10	⋯	2.538E-10
8	19	$2s^22p\ 3s\ ^1P_1^\circ$	2.27E-10 [m]	0.11E-10	2.079E-10	⋯	2.124E-10
8	20	$2p^4\ ^3P_2$	1.66E-10 [i]	0.10E-10	1.647E-10	⋯	1.636E-10
8	23	$2s^22p\ 3p\ ^1P_1$	7.5E-09 [n]	⋯	8.136E-09	⋯	8.679E-09
8	25	$2s^22p\ 3p\ ^3D_2$	**4.67E-09** [o]	0.23E-09	5.325E-09	⋯	5.314E-09
8	27	$2s^22p\ 3p\ ^3S_1$	**2.9E-09** [p]	0.2E-09	2.330E-09	⋯	2.362E-09
8	28	$2p^4\ ^1D_2$	4.25E-10 [i]	0.14E-10	4.227E-10	⋯	4.191E-10
8	30	$2s^22p\ 3p\ ^3P_1$	3.03E-09 [o]	0.18E-09	2.877E-09	⋯	2.928E-09
8	32	$2s^22p\ 3p\ ^1D_2$	3.50E-09 [q]	0.12E-09	3.316E-09	⋯	3.428E-09
8	33	$2s^22p\ 3p\ ^1S_0$	1.78E-09 [q]	0.38E-09	1.637E-09	⋯	1.684E-09
8	36	$2s^22p\ 3d\ ^1D_2^\circ$	**1.7E-10** [i]	0.3E-10	1.405E-10	⋯	1.427E-10
8	37	$2s^22p\ 3d\ ^3F_4^\circ$	5.0E-09 [q]	0.5E-09	5.144E-09	⋯	5.160E-09
8	49	$2p^4\ ^1S_0$	1.5E-10 [i]	0.2E-10	1.658E-10	⋯	1.641E-10

Notes. The experimental lifetimes are highlighted in boldface when their differences with the MCDHF values are larger than 10%.
[a] Experimental lifetimes and their uncertainties.
[b] The present MCDHF lifetimes.
[c] The MCDHF1 lifetimes calculated by Jönsson & Bieroń (2010), Jönsson et al. (2011).
[d] The MCHF lifetimes calculated by Tachiev & Froese Fischer (2001), Froese Fischer & Tachiev (2004).
The experimental lifetimes from [e] Träbert et al. (2000), [f] Smith et al. (2004), [g] Träbert et al. (2012), [h] Johnson et al. (1984), [i] Pinnington et al. (1974), [j] Knystautas et al. (1979), [k] McIntyre et al. (1978), [l] Buchet et al. (1978), [m] Pinnington et al. (1978), [n] Druetta et al. (1971), [o] Coetzer et al. (1986), [p] Berry & Bickel (1970), [q] Pinnington (1970).

levels are displayed as a function of the nuclear charge Z in Figure 3. Anomalies appear for the experimental lifetimes of the $2s\,2p^3\ ^3D_2^\circ$ levels in Ne V and Mg VII, and the $2s\,2p^3\ ^3P_2^\circ$ level in Ne V. By contrast, the present MCDHF values for the $2s\,2p^3\ ^3D_2^\circ$ and $2s\,2p^3\ ^3P_2^\circ$ levels vary smoothly along the isoelectronic sequence from O III to Mg VII. Since we used the same computational processes in the MCDHF calculations along the electronic sequence, the accuracy of our MCDHF lifetimes for all the ions is expected to be consistent and systematic. Therefore, large deviations ($\geqslant 10\%$) between the experimental lifetimes and the present MCDHF values for the $2s\,2p^3\ ^3D_2^\circ$ levels in Ne V and Mg VII, and the $2s\,2p^3\ ^3P_2^\circ$ level in Ne V reveal that the accuracy of the corresponding relatively early beam-foil measurements should be low. Future accurate experiments are expected to prove the above conclusion.

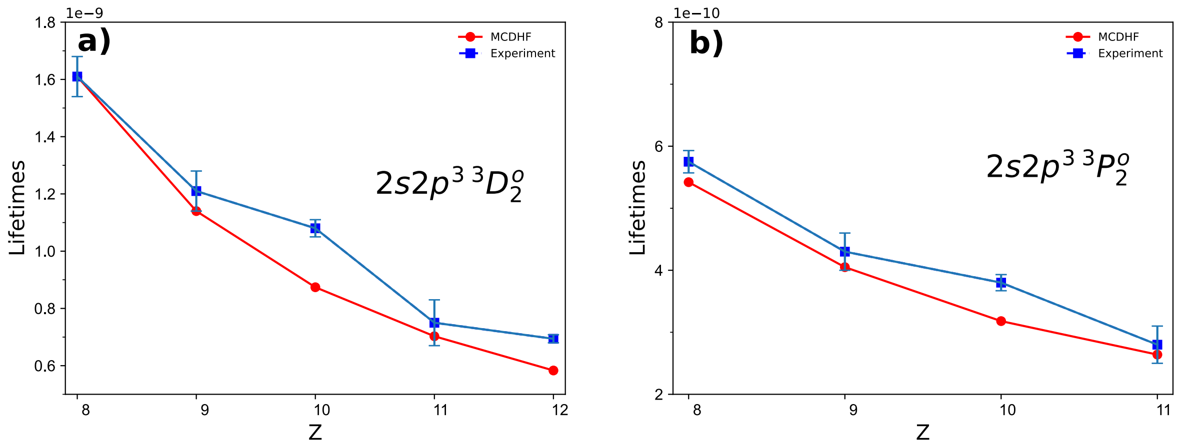

Figure 3. The experimental lifetimes (in seconds) and the present MCDHF values (in seconds) for the (a) $2s\,2p^3\ ^3D_2°$ and (b) $2s\,2p^3\ ^3P_2°$ levels are displayed as a function of the nuclear charge Z. The data for these levels are available in Table 6.

3.4. Summary

Using the MCDHF method combined with the RCI approach, calculations have been performed for the 156 (196, 215, 272, 318) lowest states of the $2s^22p^2$, $2s2p^3$, $2p^4$, $2s^22p3s$, $2s^22p3p$, $2s^22p3d$, $2s2p^23s$, $2s2p^23p$, $2s2p^23d$, $2p^33s$, $2p^33p$, $2p^33d$, $2s^22p4s$, $2s^22p4p$, $2s^22p4d$, $2s^22p4f$, $2s2p^24s$, $2s2p^24p$, $2s2p^24d$, $2s2p^24f$, $2s^22p5s$, $2s^22p5p$, $2s^22p5d$, $2s^22p5f$, and $2s^22p5g$ configurations in O III (F IV, Ne V, Na VI, Mg VII). Excitation energies, radiative lifetimes, and transition parameters are provided.

The accuracy of the MCDHF results is carefully estimated by employing comparisons with experimental data and comparisons between values calculated using different layers of the active set, as well as comparisons between values calculated using different forms, i.e., length and velocity forms. By comparing available experimental wavelengths with the MCDHF results, the previous line identifications for the $n = 5$, 4, $3 \rightarrow n = 2$ transitions of Na VI in the X-ray and EUV wavelength range are revised. For several previous identifications, discrepancies have been found. Meanwhile, tentative new (or revised) identifications have been proposed.

The present work has significantly increased the amount of accurate data for the C-like isoelectronic sequence, extending our previous calculations (Wang et al. 2014). The complete accurate data set including both energy and transition results, which fills the gap for lacking atomic data on C-like ions from O III to Mg VII, can be reliably applied to line identification and modeling purposes involving the $n > 3$ high-lying states of the C-like isoelectronic sequence. The present work can also be considered as a benchmark for other calculations.

We acknowledge the support from the National Key Research and Development Program of China under grant No. 2017YFA0402300, the National Natural Science Foundation of China (grant Nos. 12074081, 12104095, 11974080, and 11703004), the Nature Science Foundation of Hebei Province, China (A2019201300), and the Laboratory of Computational Physics of Institute of Applied Physics and Computational Mathematics (grant No. HX0202/-20). This work is also supported by the Fonds de la Recherche Scientifique—(FNRS) and the Fonds Wetenschappelijk Onderzoek—Vlaanderen (FWO) under EOS Project No. O022818F, and by the Swedish research council under contract 2016-04185. GDZ acknowledges support from STFC (UK) via the consolidated grant ST/T000481/1 to the solar/atomic astrophysics group, DAMTP, University of Cambridge. KW expresses his gratitude for the support from the visiting researcher program at Fudan University.

Software: GRASP2K (Jönsson et al. 2007, 2013) and CHIANTI (Dere et al. 1997; Del Zanna et al. 2021) are used in the present work.

ORCID iDs

G. Gaigalas https://orcid.org/0000-0003-0039-1163
L. Radžiūtė https://orcid.org/0000-0003-2140-9924
K. Wang https://orcid.org/0000-0001-6998-1693

References

Aggarwal, K. M., Hibbert, A., & Keenan, F. P. 1997, ApJS, 108, 393
Aggarwal, K. M., & Keenan, F. P. 1999, ApJS, 123, 311
Aggarwal, K. M., Keenan, F. P., & Msezane, A. Z. 2001, ApJS, 136, 763
Al-Modlej, A., Alraddadi, R. A. B., & Nessib, N. B. 2018, EPJP, 133, 379
Badnell, N. R. 1997, JPhB, 30, 1
Beiersdorfer, P., & Träbert, E. 2018, ApJ, 854, 114
Berry, H. G., & Bickel, W. S. M. I. W. R. J. W. R. E. 1970, ApL, 5, 81
Bhatia, A., & Doschek, G. 1993, ADNDT, 55, 315
Bhatia, A., & Doschek, G. 1995, ADNDT, 60, 145
Brooks, D. H., Fischbacher, G. A., Fludra, A., et al. 1999, A&A, 347, 277
Buchet, J.-P., Buchet-Poulizac, M.-C., & Druetta, M. 1978, PhyS, 18, 496
Coetzer, F., Kotzé, T., Mostert, F., & van der Westhuizen, P. 1986, AcSpe, 41, 847
Cowan, R. D. 1981, The Theory of Atomic Structure and Spectra (Berkeley, CA: Univ. California Press)
Curdt, W., Brekke, P., Feldman, U., et al. 2001, A&A, 375, 591
Curdt, W., Feldman, U., Laming, J. M., et al. 1997, A&AS, 126, 281
Curdt, W., Landi, E., & Feldman, U. 2004, A&A, 427, 1045
Dean, C. A., & Bruhweiler, F. C. 1985, ApJS, 57, 133
Del Zanna, G., & Andretta, V. 2011, A&A, 528, A139
Del Zanna, G., Dere, K. P., Young, P. R., & Landi, E. 2021, ApJ, 909, 38
Del Zanna, G., & Mason, H. E. 2018, LRSP, 15, 5
Del Zanna, G., & Woods, T. N. 2013, A&A, 555, A59
Delamere, P. A., Bagenal, F., & Steffl, A. 2005, JGR, 110, A12223
Dere, K. P., Landi, E., Mason, H. E., Monsignori Fossi, B. C., & Young, P. R. 1997, A&AS, 125, 149
Doschek, G. A., & Bhatia, A. K. 1990, ApJ, 358, 338
Druetta, M., Poulizac, M. C., & Dufay, M. 1971, JOSA, 61, 515
Dyall, K., Grant, I., Johnson, C., Parpia, F., & Plummer, E. 1989, CoPhC, 55, 425
Eissner, W., Jones, M., & Nussbaumer, H. 1974, CoPhC, 8, 270
Fawcett, B. 1987, ADNDT, 37, 367
Feldman, U., Behring, W. E., Curdt, W., et al. 1997, ApJS, 113, 195
Feldman, U., Curdt, W., Landi, E., & Wilhelm, K. 2000, ApJ, 544, 508
Feuchtgruber, H., Lutz, D., Beintema, D. A., et al. 1997, ApJ, 487, 962
Forrest, W. J., McCarthy, J. F., & Houck, J. R. 1980, ApJL, 240, L37

Froese Fischer, C., Godefroid, M., Brage, T., Jönsson, P., & Gaigalas, G. 2016, JPhB, 49, 182004
Froese Fischer, C., & Tachiev, G. 2004, ADNDT, 87, 1
Gaigalas, G., Froese Fischer, C., Rynkun, P., & Jönsson, P. 2017, Atoms, 5, 6
Gu, M. F. 2005, ADNDT, 89, 267
Johnson, B. C., Smith, P. L., & Knight, R. D. 1984, ApJ, 281, 477
Jönsson, P., & Bieroń, J. 2010, JPhB, 43, 074023
Jönsson, P., Gaigalas, G., Bieroń, J., Froese Fischer, C., & Grant, I. P. 2013, CoPhC, 184, 2197
Jönsson, P., He, X., Froese Fischer, C., & Grant, I. 2007, CoPhC, 177, 597
Jönsson, P., Rynkun, P., & Gaigalas, G. 2011, ADNDT, 97, 648
Kallman, T. R., & Palmeri, P. 2007, RvMP, 79, 79
Knystautas, E., Buchet-Poulizac, M. C., Buchet, J. P., & Druetta, M. 1979, JOSA, 69, 474
Kramida, A. 2013, Fusion Sci. Technol., 63, 313
Kramida, A. 2014, ApJS, 212, 11
Kramida, A., Ralchenko, Yu., Reader, J. & NIST ASD Team 2020, NIST Atomic Spectra Database v5.8 (Gaithersburg, MD: National Institute of Standards and Technology) https://physics.nist.gov/asd
Liu, H., Jiang, G., Hu, F., et al. 2013, ChPhB, 22, 073202
Mao, J., Badnell, N. R., & Del Zanna, G. 2020, A&A, 634, A7
McIntyre, L. C., Donahue, D. J., & Bernstein, E. M. 1978, PhyS, 17, 5
McKenna, F. C., Keenan, F. P., Hambly, N. C., et al. 1997, ApJS, 109, 225
Oliva, E., Pasquali, A., & Reconditi, M. 1996, A&A, 305, L21
Olsen, J., Roos, B. O., Jørgensen, P., & Jensen, H. J. A. 1988, JChPh, 89, 2185
Parenti, S., Vial, J.-C., & Lemaire, P. 2005, A&A, 443, 679
Pettersson, S.-G. 1982, PhyS, 26, 296
Pinnington, E. 1970, NucIM, 90, 93
Pinnington, E. H., Donnelly, K. E., Kernahan, J. A., & Irwin, D. J. G. 1978, CaJPh, 56, 508
Pinnington, E. H., Irwin, D. J. G., Livingston, A. E., & Kernahan, J. A. 1974, CaJPh, 52, 1961
Raassen, A. J. J., Mewe, R., Audard, M., et al. 2002, A&A, 389, 228
Raassen, A. J. J., & Pollock, A. M. T. 2013, A&A, 550, A55
Safronova, U. I., Ralchenko, Yu., Murakami, I., Kato, T., & Kato, D. 2006, PhyS, 73, 143
Sansonetti, J. E. 2008, JPCRD, 37, 1659
Sharpee, B., Baldwin, J. A., & Williams, R. 2004, ApJ, 615, 323
Shestov, S., Reva, A., & Kuzin, S. 2014, ApJ, 780, 15
Si, R., Li, S., Guo, X. L., et al. 2016, ApJS, 227, 16
Si, R., Zhang, C. Y., Cheng, Z. Y., et al. 2018, ApJS, 239, 3
Smith, S. J., Čadež, I., Chutjian, A., & Niimura, M. 2004, ApJ, 602, 1075
Söderqvist, J. 1946, Ark. Mat. Astron. Fys., 32A, 1
Song, C. X., Zhang, C. Y., Wang, K., et al. 2021, ADNDT, 138, 101377
Sturesson, L., Jönsson, P., & Froese Fischer, C. 2007, CoPhC, 177, 539
Sun, Y., Hu, F., Li, W., et al. 2020, ZNatA, 76, 1
Sun, Y., Hu, F., Sang, C., et al. 2018, JQSRT, 217, 388
Tachiev, G., & Froese Fischer, C. 2001, CaJPh, 79, 955
Tayal, S. S., & Zatsarinny, O. 2017, ApJ, 850, 147
Thomas, R. J., & Neupert, W. M. 1994, ApJS, 91, 461
Tian, H., Curdt, W., Teriaca, L., Landi, E., & Marsch, E. 2009, A&A, 505, 307
Träbert, E., Beiersdorfer, P., Brickhouse, N. S., & Golub, L. 2014a, ApJS, 215, 6
Träbert, E., Beiersdorfer, P., Brickhouse, N. S., & Golub, L. 2014b, ApJS, 211, 14
Träbert, E., Calamai, A. G., Gillaspy, J. D., et al. 2000, PhRvA, 62, 022507
Träbert, E., Grieser, M., von Hahn, R., et al. 2012, NJPh, 14, 023061
Wang, K., Chen, Z. B., Si, R., et al. 2016a, ApJS, 226, 14
Wang, K., Chen, Z. B., Zhang, C. Y., et al. 2018a, ApJS, 234, 40
Wang, K., Guo, X. L., Liu, H. T., et al. 2015, ApJS, 218, 16
Wang, K., Jönsson, P., Ekman, J., et al. 2017, ApJS, 229, 37
Wang, K., Li, D. F., Liu, H. T., et al. 2014, ApJS, 215, 26
Wang, K., Si, R., Dang, W., et al. 2016b, ApJS, 223, 3
Wang, K., Song, C. X., Jönsson, P., et al. 2018b, ApJ, 864, 127
Young, P. R., Dupree, A. K., Espey, B. R., & Kenyon, S. J. 2006, ApJ, 650, 1091
Young, P. R., Dupree, A. K., Espey, B. R., Kenyon, S. J., & Ake, T. B. 2005, ApJ, 618, 891
Young, P. R., Feldman, U., & Lobel, A. 2011, ApJS, 196, 23
Zeng, J., Li, Y., Liu, P., Gao, C., & Yuan, J. 2017, A&A, 605, A32
Zhang, H. L., & Sampson, D. H. 1996, ADNDT, 63, 275